Overview and Applications of the New York State Mesonet Profiler Network

BHUPAL SHRESTHA,[a,b] J. A. BROTZGE,[b] J. WANG,[b,c] N. BAIN,[b] C. D. THORNCROFT,[a,b,c] E. JOSEPH,[a,d] J. FREEDMAN,[a] AND S. PEREZ[b]

[a] *Atmospheric Sciences Research Center, University at Albany, State University of New York, Albany, New York*
[b] *New York State Mesonet, University at Albany, State University of New York, Albany, New York*
[c] *Department of Atmospheric and Environmental Sciences, University at Albany, State University of New York, Albany, New York*
[d] *National Center for Atmospheric Research, Boulder, Colorado*

(Manuscript received 2 June 2021, in final form 1 October 2021)

ABSTRACT: Vertical profiles of atmospheric temperature, moisture, wind, and aerosols are essential information for weather monitoring and prediction. Their availability, however, is limited in space and time because of the significant resources required to observe them. To fill this gap, the New York State Mesonet (NYSM) Profiler Network has been deployed as a national testbed to facilitate the research, development, and evaluation of ground-based profiling technologies and applications. The testbed comprises 17 profiler stations across the state, forming a long-term regional observational network. Each profiler station comprises a ground-based Doppler lidar, a microwave radiometer (MWR), and an environmental Sky Imager–Radiometer (eSIR). Thermodynamic profiles (temperature and humidity) from the MWR, wind and aerosol profiles from the Doppler lidar, and solar radiance and optical depth parameters from the eSIR are collected, processed, disseminated, and archived every 10 min. This paper introduces the NYSM Profiler Network and reviews the network design and siting, instrumentation, network operations and maintenance, data and products, and some example applications that highlight the benefits of the network. Some sample applications include improved situational awareness and monitoring of the sea–land breeze, long-range wildfire smoke transport, air quality ($PM_{2.5}$ and aerosol optical depth) and boundary layer height. Ground-based profiling systems promise a path forward for filling a critical gap in the U.S. observing system with the potential to improve analysis and prediction for many weather-sensitive sectors, such as aviation, ground transportation, health, and wind energy.

SIGNIFICANCE STATEMENT: The New York State Mesonet (NYSM) Profiler Network enables routine measurement of aboveground weather data and products to monitor weather and air quality across the state at high resolutions. The NYSM Profiler Network provides real-time vertical profile information to users across the emergency management, aviation, utility, and public health sectors, including NOAA and NASA, for operations and research, filling a critical gap in monitoring the low-level atmosphere. These data have been used to improve situational awareness and monitor boundary layer dynamics, sea-land breeze development, precipitation type, and air quality. Most important, the NYSM Profiler Network provides a national testbed for the creation and evaluation of new ground-based profiling instrumentation and products.

KEYWORDS: Instrumentation/sensors; Lidars/lidar observations; Microwave observations; Profilers, atmospheric; Remote sensing; Air quality; Boundary layer

1. Introduction

Thorough monitoring of the atmospheric column is an essential element in reproducing accurate weather analysis and forecasts. The World Meteorological Organization (WMO) has identified the vertical profiles of winds, temperature, humidity, and aerosols at high spatial and temporal resolution as critical atmospheric variables for high-resolution numerical weather prediction (NWP) models (WMO 2018). Yet few sensing systems can provide these much-needed data regularly. Despite their relative sparsity, radiosondes collect such vertical profile data and thus are found to be among the most valuable inputs to NWP model assimilation systems (Laroche and Sarrazin 2013). Air quality monitoring, wind energy production, aviation hazard avoidance, and weather warning operations are especially sensitive to the accuracy and resolution of the aboveground weather data, and particularly so from within the planetary boundary layer (PBL; the lowest few kilometers above the surface). Whereas surface networks are common across the United States and Europe, they fail to capture aboveground thermodynamic and transport processes that are critical for understanding PBL dynamics and NWP. Because of their relatively high cost, real-time observations of atmospheric profiles remain sparse, although they are an increasingly important component of NWP initialization (Illingworth et al. 2019). Satellites provide global coverage, but the temporal and spatial resolutions of such measurements are coarse, and routine satellite monitoring of the PBL is impeded by cloud cover. The National Weather Service (NWS) radiosonde network provides profiles of temperature, humidity, and wind speed and direction at high resolutions in the vertical, but because they are routinely launched only 2 times per day and are spaced hundreds of kilometers apart, they are not suitable for the continuous and dense profiling necessary for most NWP and other atmospheric modeling applications.

In 2009, a National Research Council (2009) report recommended, "As a high infrastructure priority, federal agencies and their partners should deploy lidars and radio frequency profilers nationwide at approximately 400 sites to continually

Corresponding author: Bhupal Shrestha, bshrestha@albany.edu

DOI: 10.1175/JAMC-D-21-0104.1

monitor lower tropospheric conditions." A decade later, the NASA Earth Science and Applications Decadal Survey (NASA 2019) identified "aerosol properties, aerosol vertical profiles, and cloud properties," "3D winds in the troposphere/PBL," and "Diurnal 3D thermodynamic properties and 2D PBL structure" as observing system priorities for the decade ahead. Improved sampling of the low-level vertical structure of the atmosphere is a repeated refrain from the environmental science community.

The last few decades have seen a rapid development of commercially viable sensors for collecting automated vertical profiles, including active sensors such as lidars (Doppler, Raman, differential absorption), radars, sodars, and ceilometers and passive sensors such as microwave radiometers (Wilczak et al. 1996; Güldner and Spänkuch 2001; Munkel 2006; Cimini et al. 2011; Lee et al. 2019). Such proven technology is now hardened for long-term, remote deployment and can provide automated, routine profiles of temperature, humidity, winds, aerosols, and clouds in the troposphere throughout the day and night at high vertical and temporal resolution. To research and develop these technologies, several profiler networks have been deployed. Table 1 provides a summary of profiler networks from around the world. Nevertheless, many of these networks are limited in their period of record, spatial coverage and the number of sensors deployed, often due to the relatively high purchase and operations and maintenance costs. For example, the annualized cost for the NOAA Profiler Network (installation began in 1988) was close to $4 million at the time (Schlatter 2004), and the program was discontinued in 2014. To move forward, a dedicated, regional-scale testbed is needed to properly evaluate the robustness of profiling technologies and to better define the applications for such data before these technologies can be fully integrated into the U.S. weather observing enterprise.

To fill this critical observational gap and address the needs of NWP, operational forecasters, and researchers, the New York State Mesonet (NYSM) Profiler Network was developed. The NYSM Profiler Network (http://nysmesonet.org/networks/profiler) comprises 17 profiler stations deployed statewide (Fig. 1). Each NYSM profiler station operates a ground-based Doppler lidar, a microwave radiometer, and an environmental Sky Imager–Radiometer. The profiler system was developed with the following objectives:

1) Measure and provide continuous real-time, high-quality vertical profiles of atmospheric data—wind, aerosol backscatter,

TABLE 1. List of profiler networks around the world.

Name	Location	Stations	Sensors	Measurements
Colorado Wind Profiling Network (Strauch et al. 1983)	Colorado	5	Wind-profiling radar	Wind profile
ARM Radar Network[a] (North et al. 2017; Kollias et al. 2020)	Around the world	Over 20	Doppler, cloud, and precipitation radar	Wind profile, cloud, and precipitation
The Helsinki testbed[b] (Koskinen et al. 2011)	Southern Finland		Ceilometer, Doppler radar, radiosonde, wind profiler with RASS	Wind, aerosol backscatter, temperature, and moisture profile
DWD Ceilometer Network (Flentje et al. 2010)	Germany	52	Ceilometer	Backscatter profile
Space Science and Engineering Center (SSEC) Portable Atmospheric Research Center (SPARC) and the Collaborative Lower Atmosphere Profiling System (CLAMPS) (Wagner et al. 2019)	Mobile integrated profiling system		Atmospheric emitted radiance interferometer (AERI), Doppler lidar, high-spectral-resolution lidar (HSRL), microwave radiometer, and radiosonde	Temperature, water vapor, wind, and aerosol backscatter profile
Wind profiling radars on the U.S. West Coast (Flaherty et al. 2016)	Along the U.S. West Coast	7	Doppler radar	Wind profile
Unified Ceilometer Network (Delgado et al. 2020)	United States and Canada	32	Ceilometer	Backscatter profile
European Meteorological Network (EUMETNET) Profiling System (E-PROFILE) (Illingworth et al. 2019)	European Union nations	Over 265	Automatic lidar and ceilometer, radar wind profiler, Doppler wind lidar, and microwave radiometer	Aerosol backscatter, wind, temperature, and moisture profile

[a] ARM Southern Great Plains sites have four extended facilities with interferometer, microwave radiometer, and Doppler lidar.
[b] Only profiler sensors are considered. The testbed also has 311 surface weather stations and 44 cellular-telephone base-station masts.

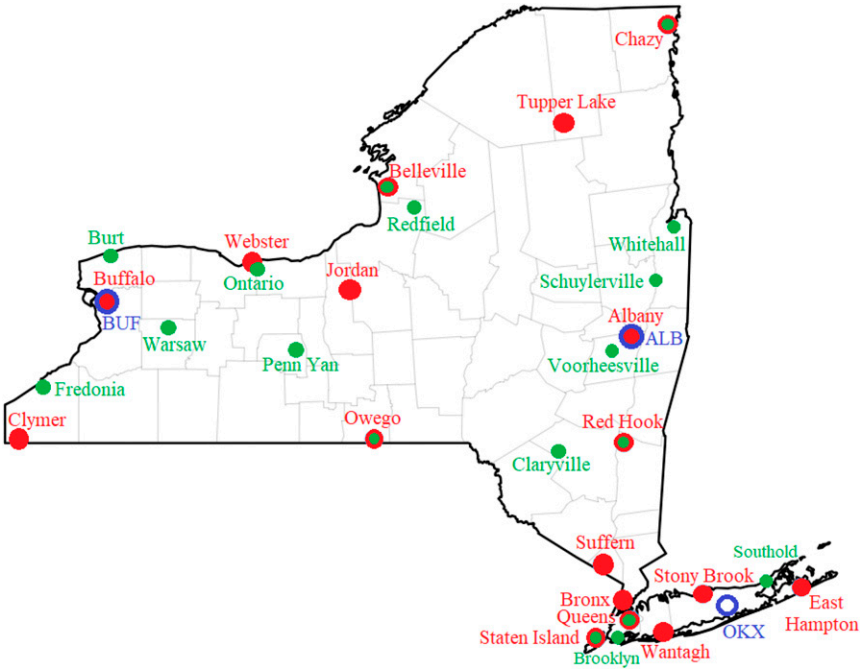

FIG. 1. The NYSM Profiler Network (red dots) and Flux Network (green dots). Blue circles represent NWS radiosonde stations.

temperature, and humidity along with spectral solar radiance and optical depth—from across New York for use in operations by multiple users, including emergency management, aviation, utilities, and researchers.

2) Create a high-quality, multiyear archive of vertical profile, flux, and atmospheric measurements for satellite remote sensing and NWP model improvement, validation, research, and development.
3) Engage a broad-based user community who can benefit from output produced by such a network.
4) Develop value-added products to expand the utility and value of the network.
5) Evaluate the economic viability of a large-scale profiler network for use in operations. Specifically, develop and implement a user-based model for financing and operating a stand-alone profiler network that is shared by the commercial, government, and academic communities.

This paper provides an overview of the NYSM Profiler Network and is organized as follows. The NYSM Profiler Network design and siting are discussed in section 2. Instrumentation is described in section 3. Network operations and maintenance are presented in section 4. Data and available products are presented in section 5. A few example applications highlighting the benefit of the network are discussed in section 6, with a summary and conclusions presented in section 7.

2. NYSM Profiler Network design and siting

The NYSM Profiler Network was configured in a way to best satisfy mesoscale measurement needs for both operational monitoring and to study predictability and improve NWP (Fig. 1). Hardware costs limited the number of stations to 17. Eleven sites were deployed around the perimeter of upstate New York to facilitate NWP model initialization by monitoring the airflow entering and exiting the state, and they were evenly distributed to maximize areal coverage. Several sites were deployed along major transportation corridors (Interstate Highways 90 and 87) or near major metropolitan areas (e.g., New York City, Buffalo, Syracuse, and Albany). Three sites are located near the three NWS radiosonde sites in New York (Buffalo, Albany, and Upton; Fig. 1). Three sites were placed on Long Island largely to monitor tropical systems and northeasters, and another three sites were triangulated around New York City (NYC) in the Bronx, Staten Island, and Queens for overlapping radar/lidar coverage to facilitate dispersion modeling. Two profiler sites are located just to the north (Suffern) and south (Wantagh) of the NYC sites for additional upwind/downwind coverage. Most of the profiler sites (except Albany, East Hampton, and Webster) are within 0.5 km of the NYSM Standard site (Brotzge et al. 2020) that provides near-surface atmospheric and soil measurements. Similarly, 6 of the 17 sites (Belleville, Chazy, Owego, Queens, Red Hook, and Staten Island) are collocated with (or very near) surface energy budget (flux) sites (Fig. 1), and they are referred to as "supersites." These sites are used to study land surface and atmospheric interactions.

Of the 17 sites, all but one (Albany) were placed on building rooftops. This provides additional security and access to utility power and communications (i.e., ethernet). Cranes were used to lift the equipment onto the roofs. Site hosts provide ready access to station equipment for regular operations and maintenance, and they receive free use of the data collected from each site. A long-term agreement was signed

between the University at Albany and the site hosts to aim at operating and maintaining the network for many years ahead for both weather and climate research in contrast to the short lifetime of past networks listed in Table 1. Most site hosts are K–12 schools (7) or universities (5); the remainder include a research institution, two wastewater treatment centers, a natural gas storage facility, and an airport. Site equipment was placed in a way that allowed as close to a full sky view as possible from each sensor. [Detailed metadata and photographs are available for each profiler site (http://nysmesonet.org/networks/profiler).]

3. Instrumentation

Each of the 17 profiler sites has a collocated Doppler lidar, microwave radiometer, and an environmental Sky Imager–Radiometer (commonly referenced as a sun photometer). As an example, the profiler site located at Albany is shown in Fig. 2.

a. WindCube 100S Doppler lidar

The WindCube 100S Doppler lidar is an active remote sensing, commercial lidar manufactured by Leosphere (now owned by Vaisala, Inc.; for specifications, see Table 2). This system is based on the WindCube technology of fibered architecture, fibered amplification, and coherent detection (Cariou et al. 2018). The flexible architecture of the system allows the user to adjust the pulse repetition frequency and pulse length to the desired measurement range and spatial resolution. A master oscillator power amplifier (MOPA) is used as a transmitter with a laser at near-infrared wavelength of 1540 nm. At this wavelength, the laser is eye safe, and transmission through the atmosphere is efficient because of negligible molecular extinction. In general, the Doppler lidar emits short laser pulses and records a small fraction of the Doppler-shifted backscattered signal from aerosols and cloud particles along the line of sight (LOS). Such backscattered signal is detected by a highly sensitive heterodyne technique (Boquet et al. 2016) to generate range resolved radial wind speed and carrier-to-noise ratio (CNR).

The CNR is a modulated signal for a signal-to-noise ratio (SNR), proportional to the backscatter signal (Boquet et al. 2016). To maximize the detection range, the emitted beam of the lidar focuses on a range that is equal to the focal length of the telescope, and hence a peak can be observed in the CNR profiles due to its focal effect. Since the lidar beam has a sensitivity that follows a Lorentzian function (Hill 2018; Yang et al. 2020), the focal effect in CNR profiles can be easily corrected. During a period with a well-mixed, relatively homogenous aerosol environment, low elevation scans are performed to estimate the fitting parameters for instrumental/telescope function using the four parameter Lorentzian function. The CNR data are then calibrated to retrieve attenuated relative backscatter β_{rel}. The details about the retrieval of β_{rel} can be found in Yang et al. (2020). The β_{rel} depends upon aerosol type and concentration and is used for aerosol and cloud observations in the atmosphere (Royer et al. 2016) and is used for applications discussed in section 6.

For 3D wind measurements, the NYSM Profiler Network Doppler lidars are configured to run in Doppler beam swinging (DBS) scan mode. This scan can be quickly reconfigured to capture opportunistic (research) or potential severe weather events (e.g., high winds) that demand other scanning configurations including fixed LOS or adjusting range–height indicator (RHI), plan position indicator (PPI), or a combination sequence of scans. In DBS scan mode, the lidar makes four LOS scans at

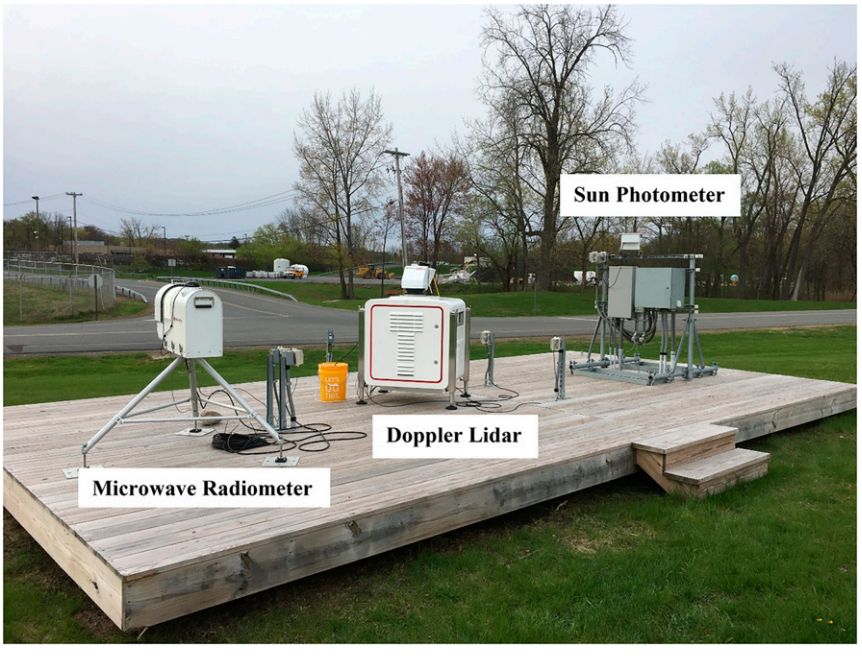

FIG. 2. The NYSM profiler site located at Albany, showing microwave radiometer, Doppler lidar, and sun photometer.

TABLE 2. The specifications of the Windcube Doppler lidar 100S.

Variable	Specification
Wavelength	1540 nm
Pulse energy	25 μJ
Pulse repetition frequency	20 kHz
Pulse length	50 m
Accumulation time	1 s
Measurement range	100–7000 m
Radial wind speed range	From −30 to +30 m s^{-1}
Wind speed accuracy	0.5 m s^{-1}
Wind direction accuracy	2°
CNR accuracy	2 dB
Scan configuration	DBS with a cycle of ~20 s
Dimensions ($L \times W \times H$)	9.95 cm × 8.10 cm × 14.10 cm
Mass	232 kg
Operating condition	
Temperature	From −25° to 45°C
Humidity	10%–100%

TABLE 3. The specifications of the microwave radiometer MP-3000.

Variable	Specification
Brightness temperature accuracy	~0.2 K
Brightness temperature range	0–400 K
Std calibrated channels	35
Surface sensor accuracy	
Temperature (From −50° to +60°C)	0.5°C at 25°C
Relative humidity	2%
Calibration types	Tip and liquid nitrogen
Measurement range	0–10 km
Temporal resolution	~2 min
Dimensions (L × W × H)	31 cm × 53 cm × 86 cm
Mass	27 kg
Operating condition	
Temperature	From −40° to +45°C
Relative humidity	0%–100%
Altitude	From −300 to 3000 m
Wind (operational/survival)	30/60 m s^{-1}

north, east, south, and west directions at an elevation angle of 75° and one LOS scan vertically, with a total scan duration of approximately 20 s. These five LOS scans are then combined to retrieve 3D wind vectors. Details of the retrieval using the DBS scan mode can be found in Newman et al. (2016) and Suomi et al. (2017).

The performance of the Doppler lidar (data availability and maximum measurement range) depends upon the aerosol type and concentration, atmospheric refractive turbulence, humidity, and precipitation (Aitken et al. 2012). The accuracy and validity of the lidar data has been tested by several studies (e.g., Kumer et al. 2014; Aitken et al. 2012; Suomi et al. 2017).

b. *Microwave radiometer*

A multichannel, passive remote sensing microwave radiometer, the MP-3000, manufactured by Radiometrics, is deployed at each NYSM profiler site (specification listed in Table 3). The microwave radiometer (MWR) measures the microwave emissions from within the vertical column; each microwave frequency corresponds to a brightness temperature using Planck's radiation equation, which are then converted collectively to a single thermodynamic profile. There are 35 standard calibrated channels that measure the brightness temperature (0–400 K) within the 22–30-GHz water vapor band (K band; 21 channels) and the 51–59-GHz oxygen band (V band; 14 channels). The accuracy of the brightness temperatures measurement is key and that depends on the quality and stability of the hardware, the accuracy and precision of the tip curve calibration and liquid nitrogen calibration, thermal stability, and noise level (Liljegren 2002; Kucher et al. 2016). The calibrated brightness temperature accuracy is around 0.2 K with long term stability of <1.0 K yr^{-1} (Radiometrics 2013).

The MWR observes atmospheric brightness temperatures at zenith and at an elevation angle of 20° above the horizon

TABLE 4. The specifications of the environmental Sky Imager–Radiometer (sun photometer).

Observation	Variable	Specification
Irradiance measurement	Channels	415, 500, 610, 670, 870, 940, and 1020 nm
	Accuracy	Absolute calibration accuracy: 4% Calibration based on Langley regression: 2%
Shadow band parameters	Blocking angle	2°
	Angular resolution	0.067°
Sky image	Field of view	180°
Environmental measurement	Air temperature	±0.1°C
	Humidity	±2%
	Air pressure	±0.12 hPa
GPS location	Position accuracy	<3 m
Measurement	Temporal resolution	5 min
Instrument	L × W × H	67.6 cm × 30 cm × 24 cm
	Shadow band radius	28 cm
	Mass	~22 kg
Operating condition	Temperature	From −30° to 50°C
	Humidity	0%–100%

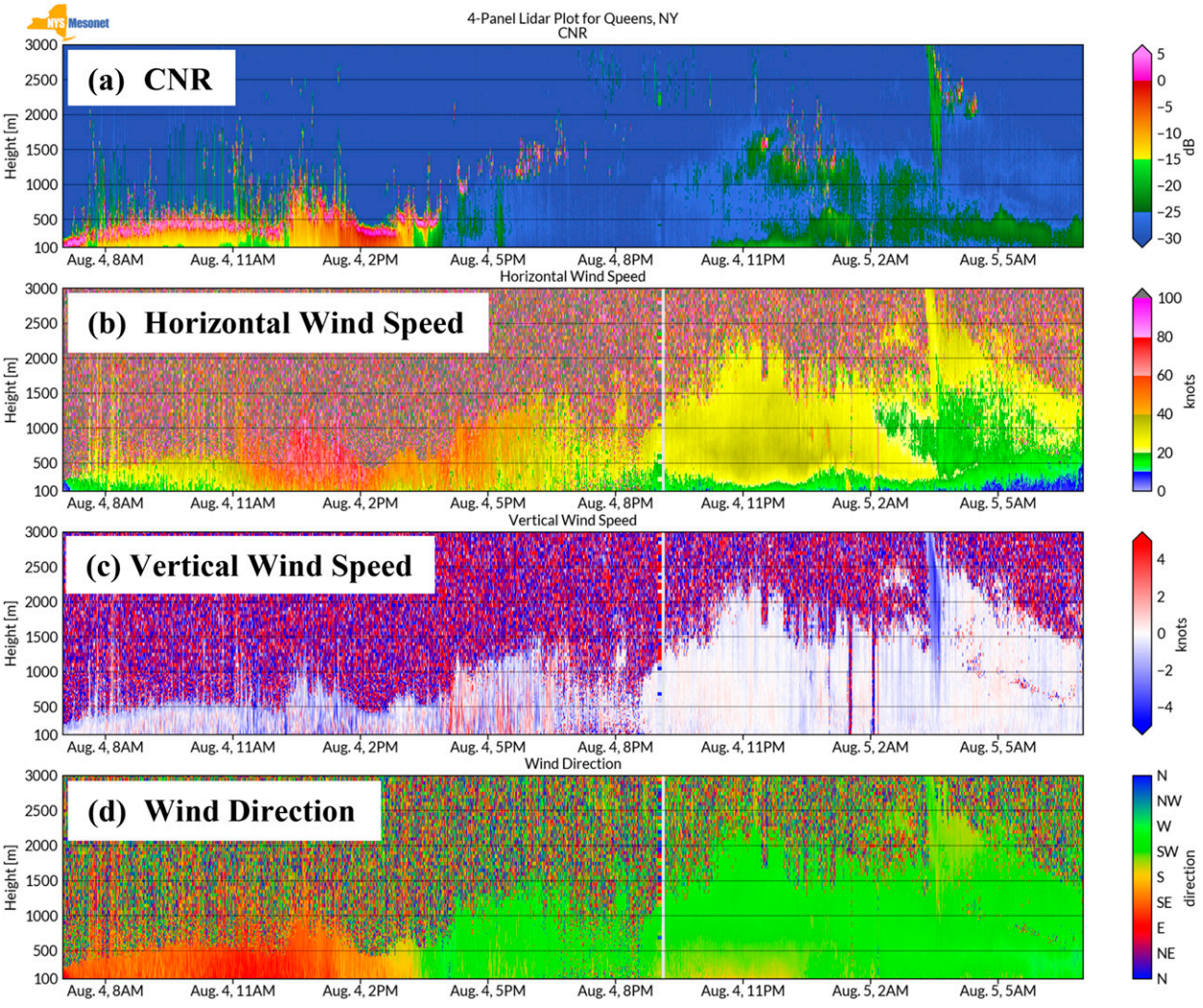

FIG. 3. Doppler lidar four-panel time–height cross-section plot for (a) CNR (dB), (b) horizontal wind speed (kt), (c) vertical wind speed (kt), and (d) wind direction (by sector) from Queens for 24 h starting at 0700 LT 4 Aug 2020.

as nominal and secondary directions. At most of the NYSM profiler sites, MWRs are oriented in such a way that the nominal direction is north, and the secondary direction is south. Profiles of temperature, relative humidity, liquid density, and vapor density up to 10 km AGL are retrieved from the brightness temperatures at those elevation angles using the radiative transfer equation (Schroeder and Westwater 1991); however, the conversion step from brightness temperatures to profile is inexact due to the limited degrees of freedom within the vertical column measurement. To compute the profiles from the brightness temperatures, the vendor applies a neural network trained with radiosonde data from a location with similar altitude and climatology to the radiometer site (Solheim et al. 1998). Prior studies suggested that the 1D variational (1DVAR) technique outperformed the neutral network method (Hewison 2007; Cimini et al. 2011). In the future, the NYSM also plans to test 1DVAR retrieval algorithm to the MWR measurements. Additional information about the instrument and retrieval algorithm can be found in Liljegren (2002), Liljegren et al. (2001), Hewison and Gaffard (2003), Bianco et al. (2017), Knupp et al. (2008), and Radiometrics (2013).

c. *eSIR (sun photometer)*

Referred to as an environmental Sky Imager–Radiometer (eSIR), this multichannel remote sensing system (specifications listed in Table 4) provides estimates of direct and diffuse radiation together with fish-eye imagery. The eSIRs were built in house by research scientists in the New York State Mesonet and Atmospheric Sciences Research Center (ASRC).

The eSIR comprises two modules: a multifilter rotating shadow-band radiometer (MFRSR), and a shaded sky imager–sun photometer. Both modules share a scanning shadow band that tracks the path of the sun throughout the day. The radiometer module has seven wavelength channels

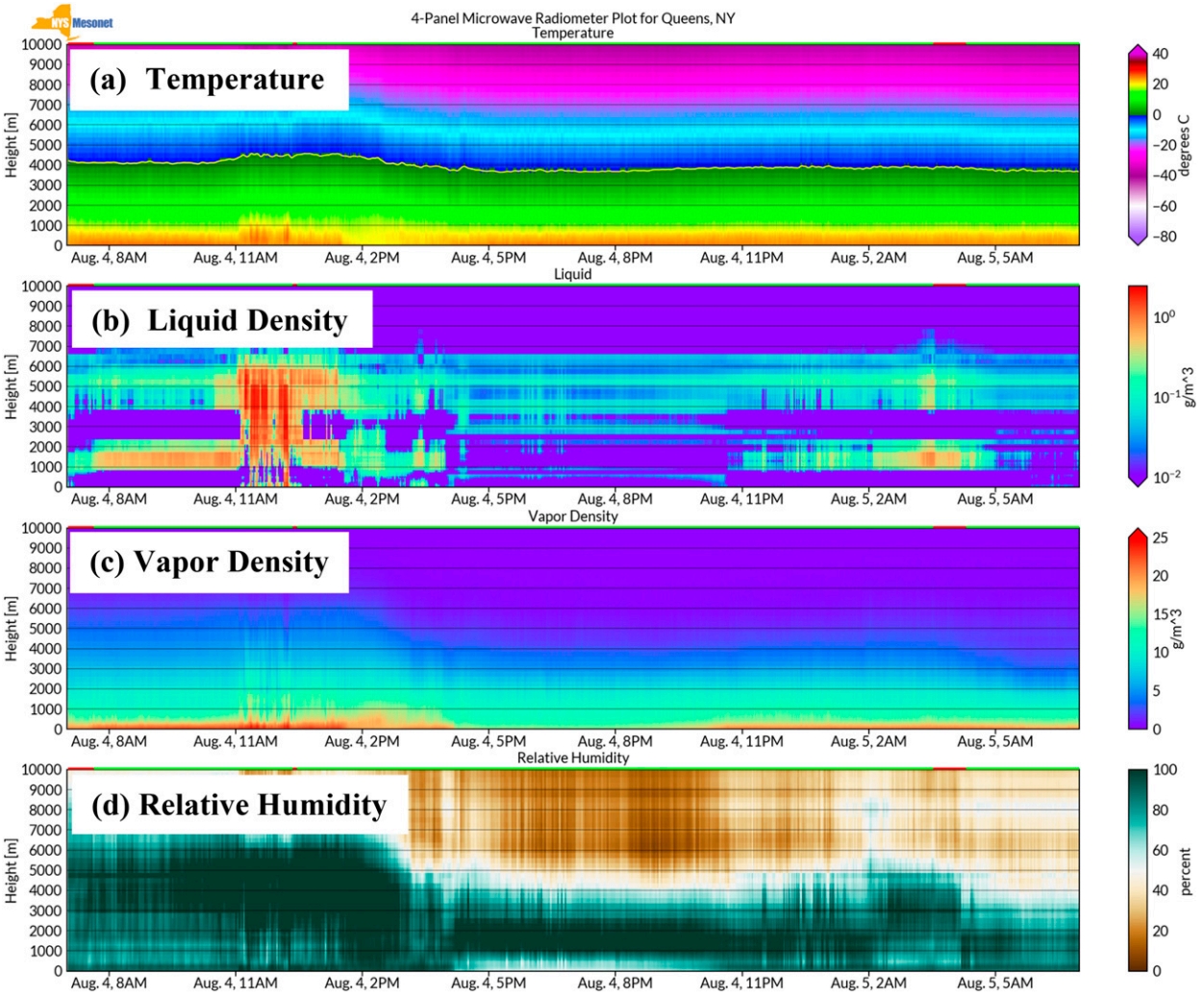

FIG. 4. Microwave radiometer four-panel time–height cross-section plot for (a) temperature (°C), (b) liquid density (g m^{-3}), (c) vapor density (g m^{-3}), and (d) relative humidity (%) from Queens for 24 h starting at 0700 LT 4 Aug 2020.

(415, 500, 610, 670, 870, 940, and 1020 nm) and uses an automated shadow-banding technique to measure narrowband spectral direct and diffuse irradiance (Yin et al. 2015). Multichannel spectral irradiances are useful in the retrieval of the optical properties of aerosol, cloud, and trace gases such as ozone, water vapor, and nitrogen dioxide in the atmosphere (Alexandrov et al. 2001; Kassianov et al. 2005; Alexandrov et al. 2008; Turner et al. 2014; Patadia et al. 2018). The sky imager module takes fish-eye sky images; a shadow band blocks the direct beam of the sun to minimize glare in sunny conditions. In addition, the eSIR also has embedded meteorological sensors that track temperature, humidity, and pressure and a GPS sensor to record the precise time and position (latitude, longitude, and elevation). All measurements are taken every 5 min during daylight hours. When the solar zenith angle is greater than 85° and during nighttime, the shadow band stops its sweeping motion and sky images are not recorded.

To measure the atmospheric aerosol properties, spectral aerosol optical depth (AOD) is retrieved using the spectral direct normal irradiances measured by the eSIR. As described in Koontz et al. (2013), AOD is estimated using the Beer–-Lambert–Bouguer Law and Langley regression. The contributing optical depth due to Rayleigh scattering and wavelength dependency on water vapor, ozone, and trace gases such as NO_2, CO_2, CH_4, and so on are considered while calculating AOD (Hansen and Travis 1974; Koontz et al. 2013; Patadia et al. 2018). Since AOD represents the measure of aerosols in the atmospheric vertical column, it is often used as a proxy to estimate surface $PM_{2.5}$ (Gupta and Christopher 2008; Schaap et al. 2009; Hu et al. 2013; Chudnovsky et al. 2014; Hua et al. 2019), particularly during well-mixed condition. The Ångstrom exponent (α; Ångström 1929) can also be derived from the AOD and is an indicator of aerosol particle size present in the atmosphere: $\alpha \leq 1$ represents coarse mode aerosols with radius ≥ 0.5 μm such as dust and sea salt, and $\alpha \geq 2$

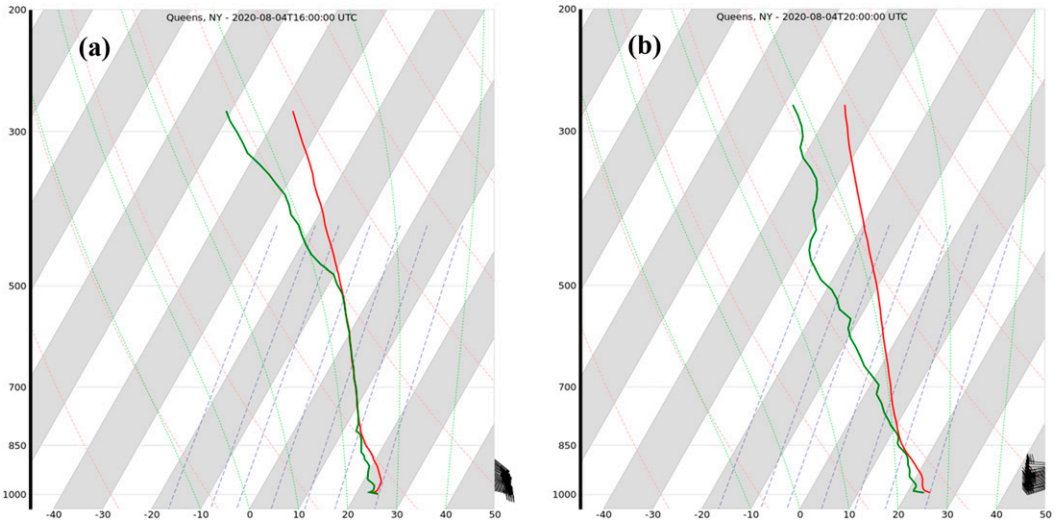

FIG. 5. Skew *T* plot generated from Doppler lidar and MWR data from Queens at (a) 1200 and (b) 1600 LT 4 Aug 2020.

represents fine mode aerosols with radius ≤0.5 μm such as urban pollution and biomass burning (Schuster et al. 2006; Eck et al. 1999). A cloud-screening technique developed by Alexandrov et al. (2004) is implemented to distinguish between clear-sky and cloudy data.

4. Network operations and maintenance

A field technician is assigned full-time to the ongoing maintenance and calibration of the NYSM Profiler Network. The technician oversees the communications, power, and sensors at each site and responds (on site or remotely) to problems as needed. While built for remote and automated operation, each sensor still requires some limited but regular maintenance. The lidar laser degrades over about a 10-yr period, and the lidar scanning head incurs significant wear and tear with time, requiring replacement after about five years of continuous use. The MWR has several degradable components that require regular replacement, including a radome, fans, and an infrared thermometer. For major sensor repairs, the MWRs are returned to the vendor, whereas a contracted technician visits the lidar for onsite repairs; the lidar's weight (>200 kg) and rooftop location make it cost prohibitive for returning it to the vendor unless major repairs are needed.

The MWR and eSIR require regular calibration. The technician visits each site every 4–6 months to calibrate the MWR. The MWR requires two types of calibrations; the calibration resets the brightness temperatures of the noise diodes for the K-band and V-band channels and hence, the quality of data depends on precision and accuracy of the calibration. A tip calibration is done remotely in the NYSM Operations Center every two weeks to reset the K band. The brightness temperature is measured at several elevation angles, and then a fitting function is applied to estimate an updated, "corrected" zenith brightness temperature (Hewison and Gaffard 2003). An in-person liquid nitrogen calibration is required for the V band every 6 months. Liquid nitrogen is poured into a polystyrene box and placed on top of the radiometer; data are collected for 30–60 min to extract a stabilized noise diode brightness temperature. Kucher et al. (2016) determined MWR calibrations are accurate within ±0.5 K. The eSIR requires instrumental recalibration about every 2 years.

5. Data and products

Data are collected from the profiler sites across the state and transmitted to servers located at the University at Albany, where the data are then quality controlled, archived, and disseminated in real time every 10 min. Extensive network, station, and sensor metadata are readily available and accessible to users through the NYSM website. The primary data available from the NYSM Profiler Network are profiles of the *u*, *v*, and *w* components of wind speed and wind direction and CNR from the Doppler lidar; profiles of temperature, relative humidity, liquid, and vapor density from the MWR; and spectral direct, diffuse, and total radiation, sky images, surface temperature, relative humidity, and atmospheric pressure from the eSIR. The combination of Doppler lidar and MWR data provides continuous profiles of winds, temperature, and moisture similar to that available from the NWS radiosonde network, but with much higher temporal resolution (every 2 min vs twice daily). The vertical resolution of the lidar data is 25 m from 100 to 1000 m and 50 m from 1000 to 7000 m with a temporal resolution of approximately 20 s for a full DBS scan. The vertical resolution of MWR data is 50 m from the surface to 500 m, 100 m from 500 to 2000 m, and 250 m from 2000 to 10000 m with a temporal resolution of approximately 2 min. The eSIR collects data over 5-min periods during daylight hours. These data are archived in NetCDF and comma-separated-values (CSV) format, and sky

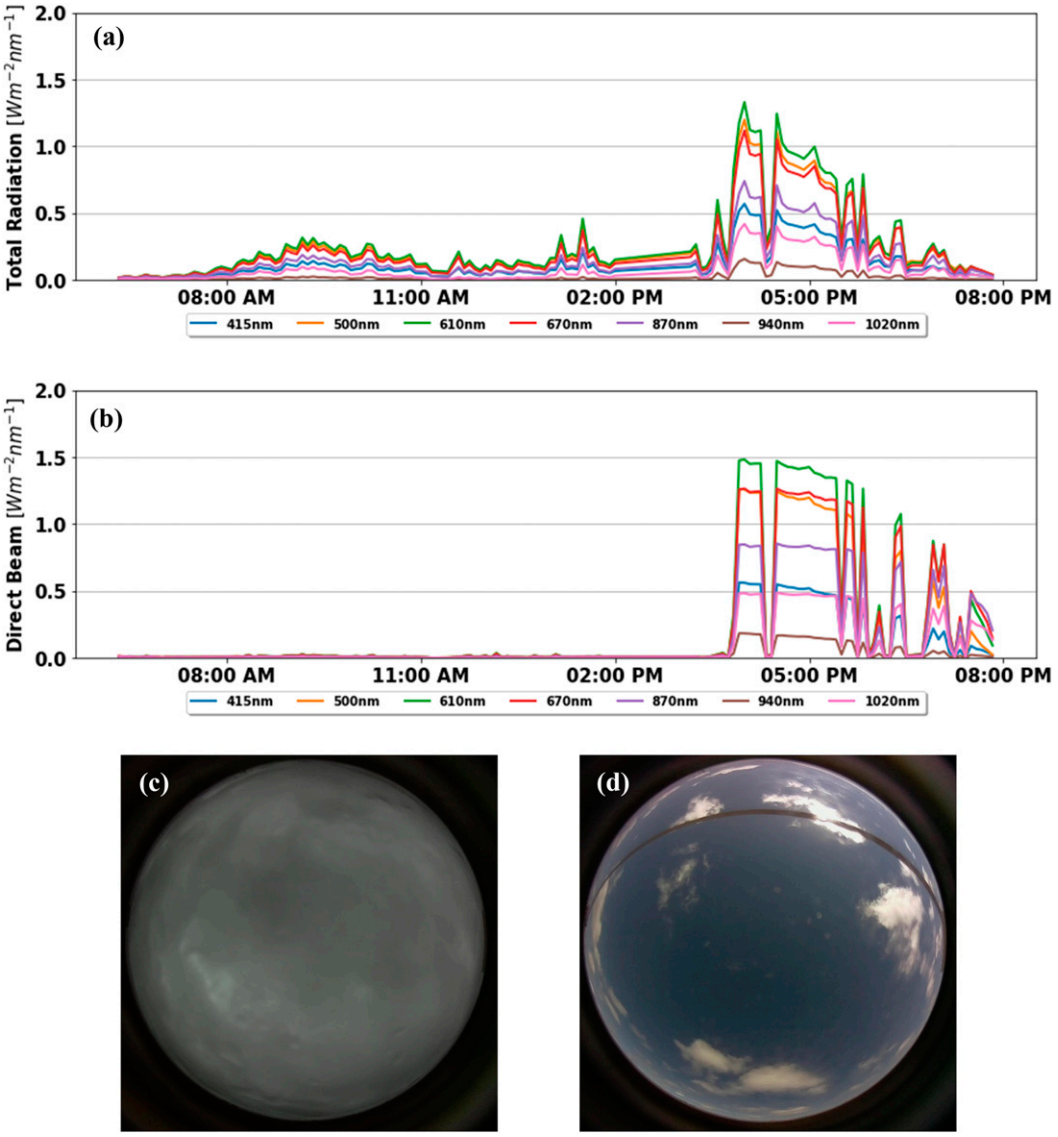

FIG. 6. Sun photometer two-panel time series plot for (a) total radiation (W m^{-2} nm^{-1}) and (b) direct normal radiation (W m^{-2} nm^{-1}) from Queens for the daylight hours on 4 Aug 2020 along with the fish-eye images at (c) 1200 LT and (d) 1600 LT.

images are provided in ".jpg" format. Data are available to users upon request at cost in accordance with NYSM Data Policy (http://www.nysmesonet.org/weather/requestdata). A "ReadMe" file explains the data file format, variables, and their units along with site and sensor information. A detailed evaluation of the Profiler Network measurement data bias with reference measurements (radiosonde and sun photometer) is presented in B. Shrestha and E. Joseph (2021, unpublished manuscript).

A real-time display showing the data collected during the last 24 h is available online (http://www.nysmesonet.org/networks/profiler) and is updated every 10 min. As an example, the 24-h four-panel time–height cross-section plots from the Doppler lidar and MWR at Queens, New York are shown in Figs. 3 and 4 Doppler lidar data are shown up to 3 km AGL. The skew T plots generated using the Doppler lidar and MWR data are shown in Fig. 5. The eSIR spectral total and direct normal radiation time series plots for daylight hours along with fish-eye sky images are shown in Fig. 6. The combination of three measurement data shown in Figs. 3–6 demonstrate the value of the NYSM Profiler Network in monitoring Tropical Storm Isaias and are discussed in detail in section 6a. Additional real-time display of derived products such as PBL height, air quality indicator ($PM_{2.5}$, AOD, and Ångstrom exponent), forecast, and stability indices are currently under development.

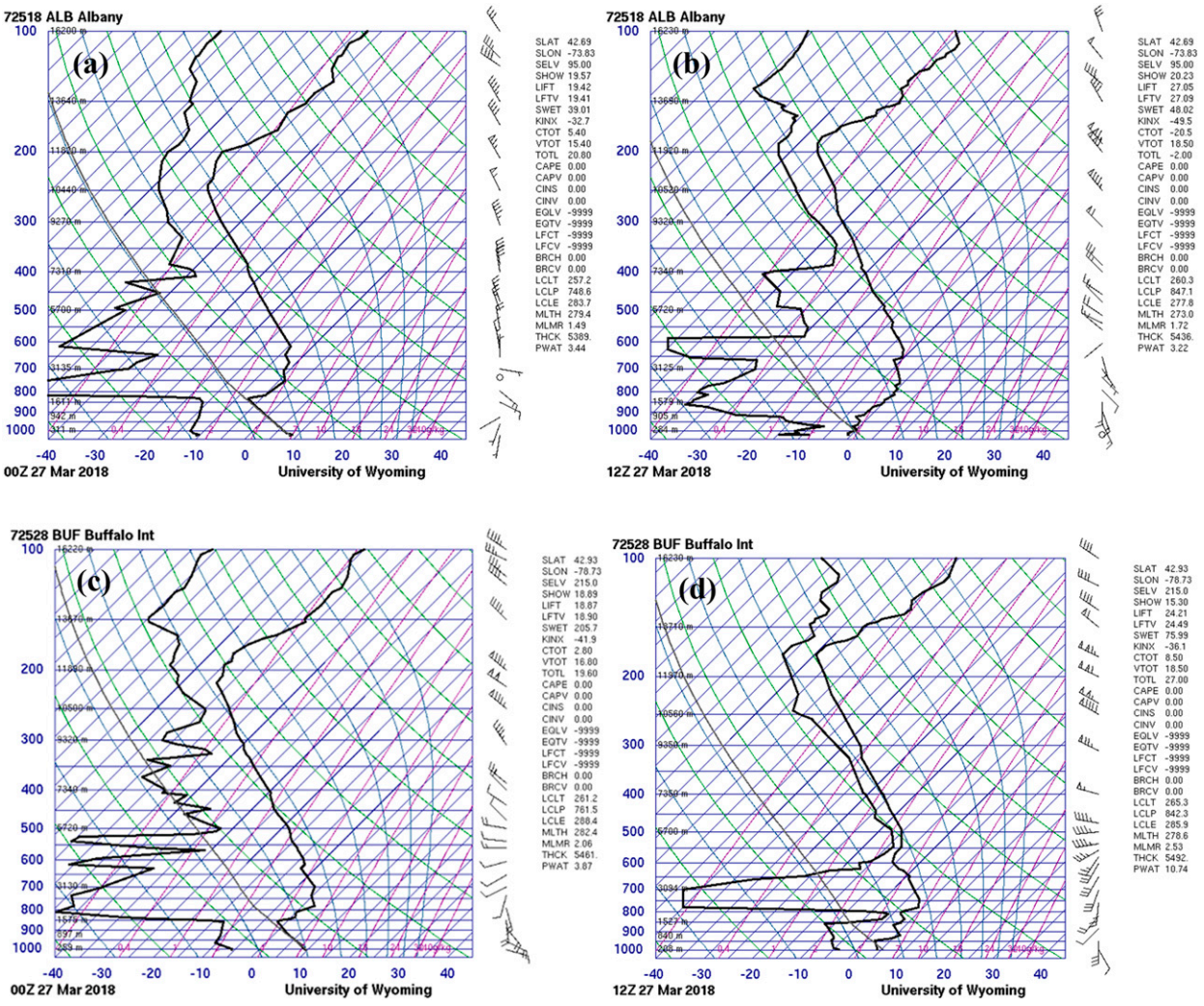

FIG. 7. Skew *T* plots for NWS radiosonde data on 27 Mar 2018: (a) Albany at 0000 UTC, (b) Albany at 1200 UTC, (c) Buffalo at 0000 UTC, and (d) Buffalo at 1200 UTC, retrieved from the University at Wyoming.

6. Example applications

As discussed in section 1, vertical profiling technology fills a noted gap in atmospheric sensing with the expectation that such data will improve NWP and enhance situational awareness for operations by supplementing the NWS radiosonde network with much greater temporal and spatial sampling. As a participant of the National Mesonet Program, the NYSM makes Profiler data available to the NWS in real time. Since the feed was established in 2018, the Profiler data have been used by regional NWS forecast offices to improve short-term forecasts of low-level wind, temperature, fog and cloud development and erosion, convective instability, precipitation onset and type. However, the integration of multiple, collocated profiling sensors—the lidar, microwave radiometer, and sun photometer—has expanded the versatility and utility of the network as well. Several examples below demonstrate some of the benefits and products that such a network can offer.

a. Improved situational awareness: High-temporal sampling

The high-temporal-resolution data of the NYSM Profiler Network can provide critical insight for emergency management operations. On 4 August 2020, the NWS issued a tornado watch that included New York City effective from 1100 until 1600 local time (LT) as Tropical Storm Isaias approached from the south. Figures 3 and 4 show the data from the Doppler lidar and MWR at Queens. Winds > 40 kt ($1 \text{ kt} \approx 0.51 \text{ m s}^{-1}$) were observed between 1100 and 1500 LT (Fig. 3b). Easterly to southeasterly winds were dominant until about 1500 LT as the tropical storm approached from the Atlantic Ocean, followed by weak westerly winds as the storm moved past and weakened (Fig. 3d). Precipitation was observed during the period as indicated by the negative vertical wind speed (Fig. 3c), the relatively high liquid density and relative humidity (Figs. 4b,d), and skew *T* plot indicating saturation up to 500 hPa at 1200 LT (Fig. 5a). By late afternoon,

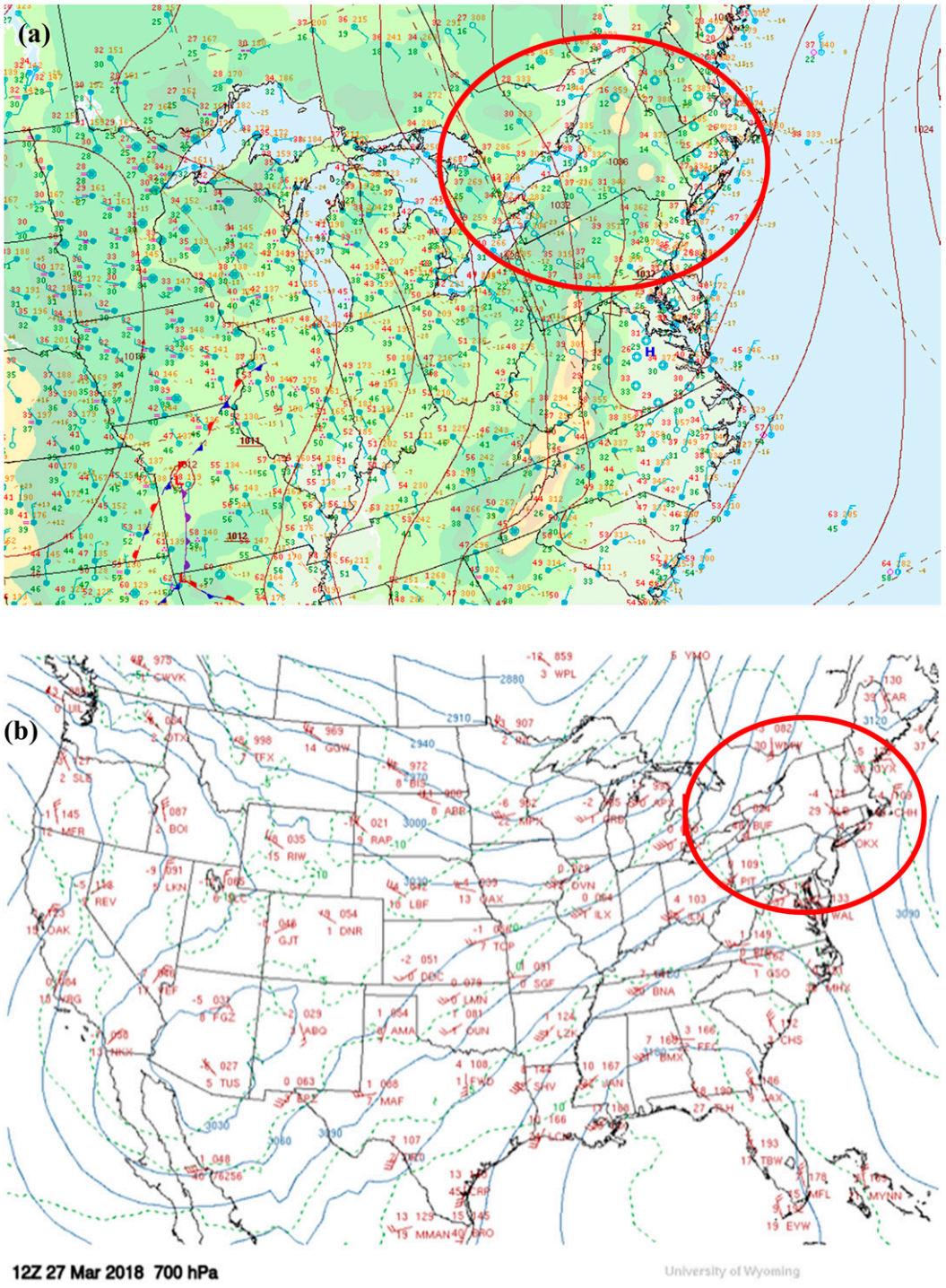

FIG. 8. (a) Surface analysis map at 0600 UTC 27 Mar 2018 retrieved from the NWS Weather Prediction Center and (b) 700-hPa map at 1200 UTC 27 Mar 2018 retrieved from the University at Wyoming. Red-outlined ovals show the New York region and its surroundings.

the sun returned with partly cloudy skies as can be seen from the increased total (Fig. 6a) and direct normal radiation (Fig. 6b) from the eSIR along with the fish-eye images during the storm at 1200 LT (Fig. 6c) and poststorm at 1600 LT (Fig. 6d). The skew T plot at 1600 (Fig. 5b) also provides evidence for the presence of clouds at around 900–800 hPa. As the sun

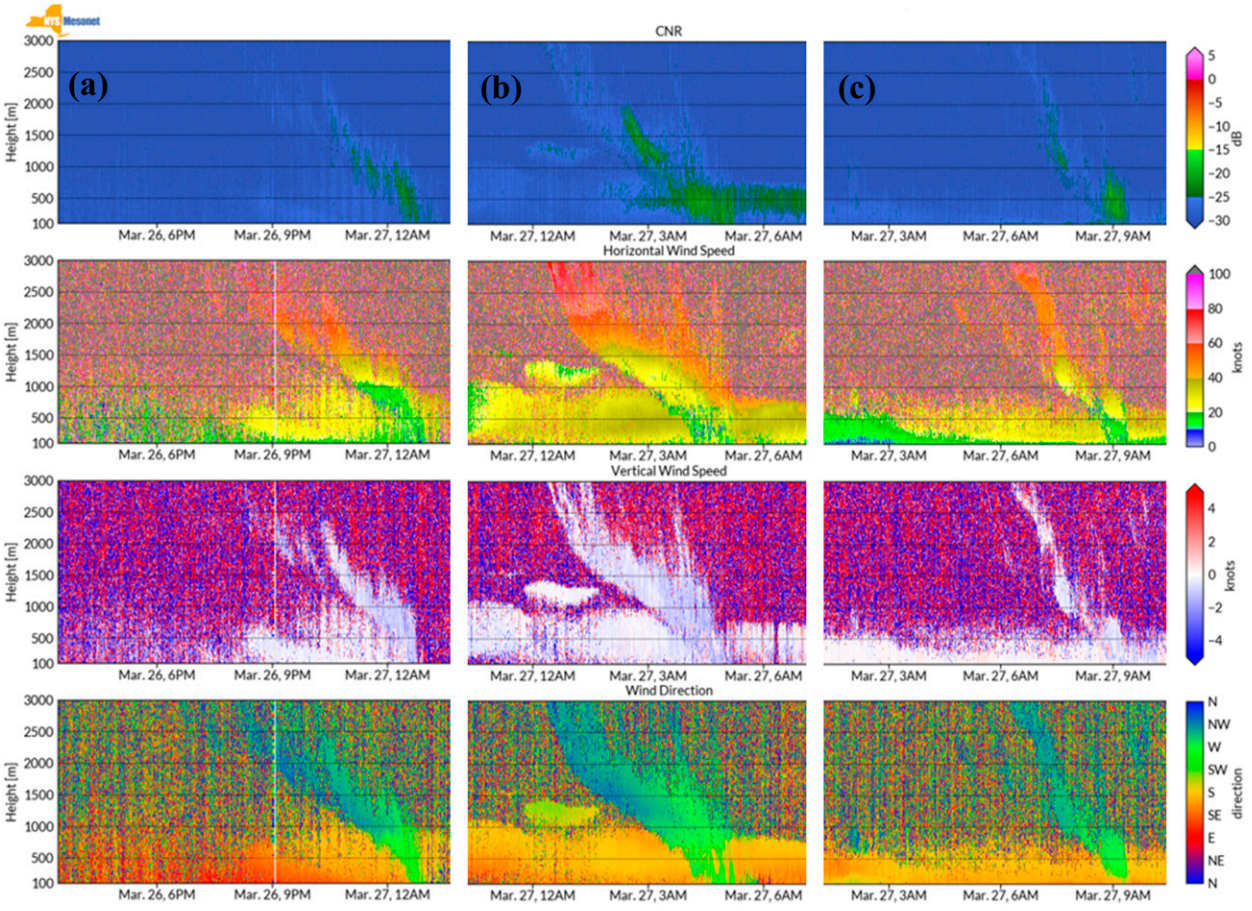

FIG. 9. Doppler lidar four-panel time–height cross-section plot for (top) CNR (dB), (top middle) horizontal wind speed (kt), (bottom middle) vertical wind speed (kt), and (bottom) wind direction (by sector) from (a) Buffalo, (b) Belleville, and (c) Chazy during 26–27 Mar 2018 (in local time).

returned, vertical mixing increased as indicated by the positive and negative vertical wind speeds measured from the Doppler lidar (Fig. 3c). The vertical wind speed can be used as a proxy to estimate mixed-layer height (e.g., thermals connected to the surface indicated by positive vertical wind speed). Low-level (boundary layer cumulus) clouds can be seen throughout the day as indicated by the higher CNR values in the pink and red colors (Fig. 3a). The high-temporal sampling of the network provides emergency managers with much-improved understanding of rapidly evolving high-impact events.

b. *Improved situational awareness: Greater spatial sampling*

The NWS radiosonde network has only three sites across New York, leaving large gaps in spatial coverage across the state. A network of profiling sensors can help fill these spatial gaps. A simple event from 26 to 27 March 2018 shows the value of such a network for its ability to track individual features in space and time. In this case, a dry upper-air disturbance moved quickly from west to east across the state, with gradual subsidence associated with the strong high pressure system. The NWS radiosonde data from Albany (ALB) and Buffalo (BUF) show extremely dry air aloft (approximately above 1500 m or below 800 hPa) on 27 March 2018 (Figs. 7a–d retrieved from http://weather.uwyo.edu/upperair/sounding.html). The surface analysis map at 0600 UTC (Fig. 8a, retrieved from https://www.wpc.ncep.noaa.gov/archives/web_pages/sfc/sfc_archive.php) shows a strong high pressure system over the northeastern United States, whereas the 700-hPa map (Fig. 8b, retrieved from http://weather.uwyo.edu/upperair/uamap.shtml) shows an unusually long southwesterly fetch of air from Baja California to western New York.

This mostly quiescent upper-air disturbance was tracked across the state by the NYSM Profiler Network. Figure 9 shows Doppler lidar data from a west-to-east transection in the north from Buffalo, Belleville, and Chazy, and Fig. 10 shows a west-to-east transection in the south from Clymer, Owego, and Staten Island (locations of these sites are shown in Fig. 1). Lidar plots from each site location are very similar, showing the air aloft gradually mixing down to the surface, but data from multiple sites can track the rapid transport of the boundary. Roughly in about 9 h, the bubble of dirtier air from the west reaches to the east (in our case: from Buffalo to Chazy and from Clymer to Staten Island) with approximate speed of 18 m s^{-1} (about 35 kt). The west-to-east movement

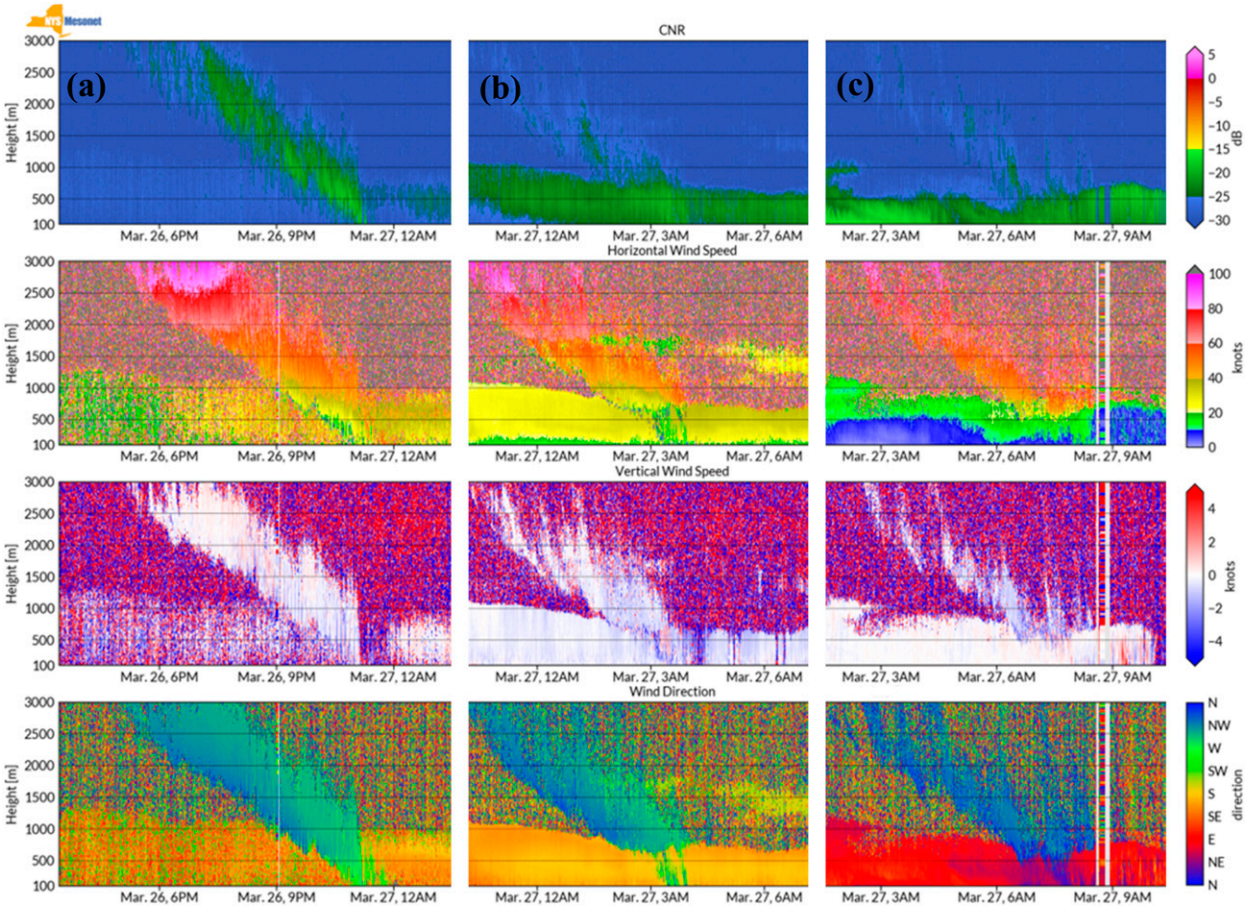

FIG. 10. As in Fig. 9, but from (a) Clymer, (b) Owego, and (c) Staten Island.

of the feature is consistent with the westerly winds aloft while the weakening of the boundary (flow becomes diluent) as it traveled easterly is consistent with subsidence. As demonstrated, large-scale networks are necessary for tracking such a feature across regional scales in real time.

c. *Ability to monitor local features*

The NYSM Profiler Network has proven beneficial for monitoring rapidly changing conditions, such as presented by the sea-breeze circulation along the Long Island (LI) coastal region in New York. Several studies (Loughner et al. 2014; Blaylock et al. 2017a; Zhang et al. 2020) have shown the contribution of sea-breeze circulation to poor air quality by increasing surface ozone concentrations in short periods around coastal areas, particularly in the summer. The six NYSM profiler stations located across NYC and LI provide a means to monitor the sea-breeze circulation and its influence on air quality around the region. For example, on 10 July 2018, ozone concentration increased from 80 ppb to over 120 ppb below 1.5 km within a 3-h period (1300–1600 LT), as measured at Flax Pond, LI (Joseph et al. 2018). Figure 11 shows the wind speed and direction from the NYSM profiler sites at Wantagh, East Hampton, and Queens, which are approximately 58 km southwest, 93 km southeast, and 75 km west from the Flax Pond, respectively. After 1000 LT, an abrupt shift in wind direction from offshore (west to northwest) to onshore (southerly) accompanied by an increase in wind speeds (from 5 to 10–20 kt) within a few hundred meters AGL can be observed at Wantagh and East Hampton. A similar trend can be observed at Queens shortly after 1200 LT. Further analysis on the identification of the sea-breeze circulation and its influence on ozone concentration are presented in Joseph et al. (2018) and Zhang et al. (2020).

d. *Ability to monitor wildfire smoke transport*

The NYSM Profiler Network has also demonstrated an ability to monitor long-range-transport smoke events. Despite a long-term downward trend in $PM_{2.5}$ and an improvement in air quality across New York (Emami et al. 2018; Rattigan et al. 2015) and the United States (Black et al. 2017), episodic events such as smoke from wildfires can cause periodic rises and adverse effects on human health. Occasionally, wildfire smoke from as far away as the western United States and Canada can affect local air quality in New York by increasing

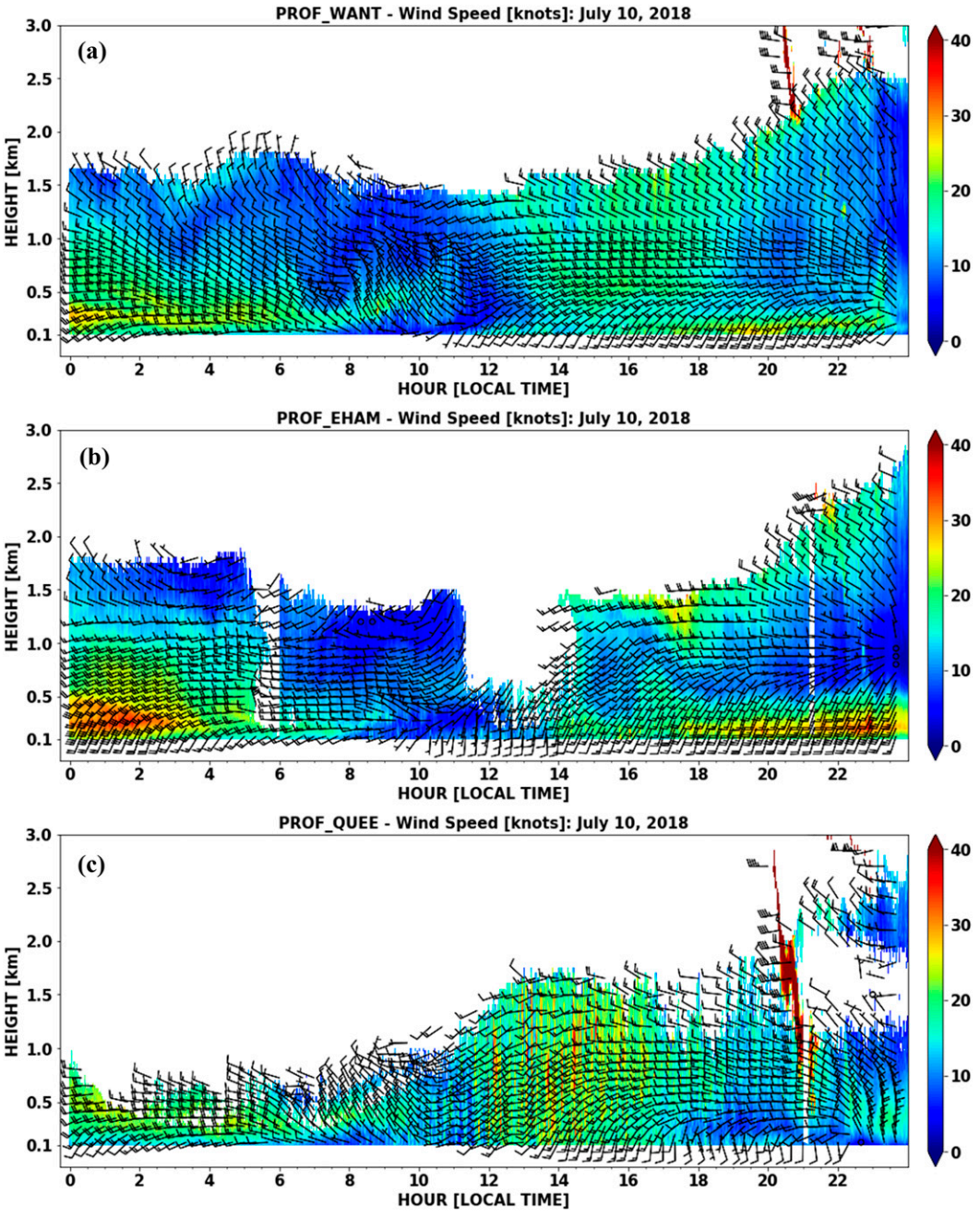

FIG. 11. Doppler lidar wind speed (kt) data overlaid with 10-min-averaged wind barbs from (a) Wantagh, (b) East Hampton, and (c) Queens for 10 Jul 2018 (in local time).

the surface $PM_{2.5}$ concentration through boundary layer entrainment and the vertical mixing process (Wu et al. 2018; Rogers et al. 2020; Hung et al. 2020). It has been speculated that the primary source of surface $PM_{2.5}$ increases in the future could be due to wildfire smoke rather than anthropogenic emissions (Ford et al. 2018; Black et al. 2017; Liu et al. 2016). Therefore, being able to monitor long-range smoke transport is important for accurate air quality monitoring, forecasting, and regulation.

One such smoke episode occurred across New York from 13 to 17 August 2018. Time series of surface $PM_{2.5}$ from Buffalo, Albany, and Queens, as monitored by the New York State Department of Environmental Conservation (NYSDEC) are shown (Fig. 12). The time series plot shows a notable increase of $PM_{2.5}$ with values rising at Buffalo beginning on 14 August, followed by rises at Albany and Queens 24 h later. Such a coincident but delayed enhancement of $PM_{2.5}$ at Albany and Queens indicates that the increases in

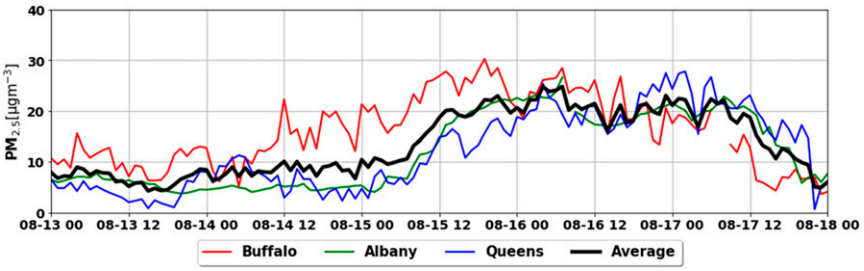

FIG. 12. Surface $PM_{2.5}$ data collected at Buffalo, Albany, and Queens by the NYSDEC during 13–17 Aug 2018 (in local time). The black line represents the average of three sites.

$PM_{2.5}$ values are not caused by local sources but are most likely due to long-range transport of smoke entering the state from the west. The smoke can be observed directly by the lidar's relative attenuated backscatter from the three NYSM profiler sites during the period of elevated $PM_{2.5}$ (Fig. 13). The strong backscatter signal of red and dark red colors represents clouds, and they are observed at all three sites during different parts of the day. The lidar shows a backscatter signal of 10^{-7}–10^{-5} m^{-1} sr^{-1} near the surface and up to 2 km at all three sites. At Buffalo, aerosols are seen aloft between 2 and 5 km starting the night of 14 August until the afternoon of 16 August. Similarly, aerosols are seen around 2 km on 15–16 August at Albany and between 2 and 4 km on 15–17 August at Queens. The aerosols at Albany and Queens are seen approximately 12–16 h later than at Buffalo. These layers of aerosols encountered subsidence and mixed into the PBL. The PBL processes of entrainment and vertical mixing provided favorable conditions to bring them down slowly to the ground causing the enhancement of $PM_{2.5}$ seen in the NYSDEC time series in Fig. 12.

Smoke can also be identified using the eSIR; here, the AOD at 500, 670, and 870 nm and Ångstrom exponent (based on 500 and 870 nm) were derived using the eSIRs at Buffalo and Queens (Fig. 14; the eSIR at Albany was not active at that time). For all three channels, AOD values greater than 0.2 and Ångstrom exponents in the range of 1.5–2 provide evidence for the presence of fine mode aerosols such as pollution or smoke. However, since urban pollution is typically found within the boundary layer, aerosols as seen from lidar backscatter above 2 km can be classified as smoke plumes. Such aloft aerosols are also evident overnight and in early morning, which therefore provide additional evidence for the smoke plume. Further evidence for the smoke plumes, their source, trajectories of transport, and detailed analysis of this smoke episode and its effect on air quality are presented in Hung et al. (2020).

e. *Ability to monitor air quality*

A fifth example demonstrates the value of the NYSM Profiler Network for the estimation of aerosol mass concentration, in terms of $PM_{2.5}$. A remote sensing technique can be used to combine the aerosol backscatter with meteorological data (B. Shrestha and E. Joseph 2021, unpublished manuscript). This nonlinear regression model is applied to data during the warm months from May to September of the years 2017–20 from Queens, New York. Data from the years 2017–19 are used for fitting the model, and then tested on data from 2020. Relative backscatter data are obtained from the NYSM Doppler lidar; temperature, relative humidity and wind speed data are collected from the coincident NYSM standard site—both located at Queens and $PM_{2.5}$ data are obtained from the NYS DEC air quality monitoring site at Queens College. The NYSM site is about 1 km away from the NYS DEC site. All data are averaged hourly and are selected based on the availability of Doppler lidar data. Values retrieved from the nonlinear model are compared with the surface measured $PM_{2.5}$ (Fig. 15). The slope and y intercept are 0.84 and 1.32, respectively. The coefficient of determination R^2 and root-mean-square error (RMSE) are found to be 0.70 and 2.30 $\mu g\ m^{-3}$, respectively. Applying an F test, the p value is below 0.05 (standard significance level) yielding a corresponding confidence level of 95%. The nonlinear model continues to be evaluated at other sites along with its application on vertical profiling of $PM_{2.5}$.

f. *Ability to monitor PBL height*

The NYSM Profiler Network can be used to monitor PBL height. The lidar has become a powerful tool in the detection of PBL height due to its continuous measurement, broad measurement range, and high vertical and temporal resolution. Several lidar techniques have been developed for estimating PBL height; three common approaches include the gradient, variance, and wavelet covariance transform (WCT) methods. The gradient and variance methods assume the PBL height corresponds to the minimum gradient and maximum variance in the relative attenuated backscatter. The WCT method (Brooks 2003; Baars et al. 2008; Granados-Munoz et al. 2012) assumes a higher concentration of aerosols within the PBL with a steep decrease in concentration in the free troposphere above. The sharp transition zone (largest gradient) of the lidar signal change is considered to be the PBL height, usually near the center of the entrainment layer. Using these three techniques, PBL heights are retrieved from Doppler lidar and are compared with PBL heights estimated from a nearby NWS radiosonde using the Heffter method (Heffter 1980; Sivaraman et al. 2013) and from the High-Resolution

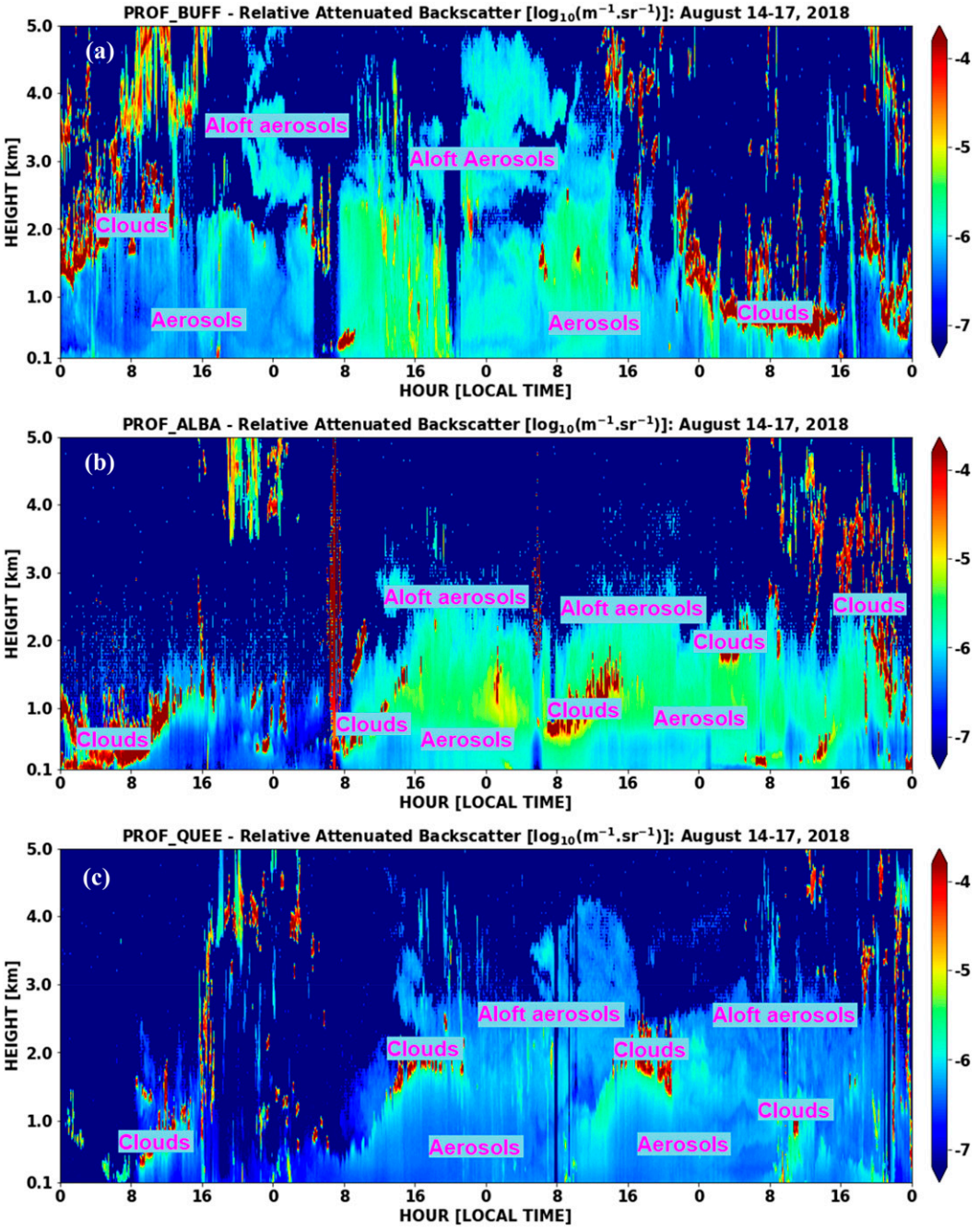

FIG. 13. Doppler lidar relative attenuated backscatter data from (a) Buffalo, (b) Albany, and (c) Queens during 14–17 Aug 2018 (in local time).

Rapid Refresh (HRRR; Blaylock et al. 2017b, https://rapidrefresh.noaa.gov/hrrr/) model, shown in Fig. 16.

Retrieved PBL heights for 22 June 2020 are plotted for Buffalo (Fig. 16a), Albany (Fig. 16b), and Queens (Fig. 16c). At Buffalo (Fig. 16a), the variance and gradient method fail to detect PBL height in the presence of complex aerosol layers between 0600 and 1200 LT and after 1700 LT when the residual layer starts to develop. The WCT and HRRR model show good agreement with each other for most of the day. The WCT also shows good agreement with the radiosonde at both launch times. At Albany, (Fig. 16b), all three lidar methods show good agreement throughout the day except during 0600–0900 LT when the gradient and variance method are affected by the presence of the residual layer. The WCT and HRRR model are consistent in capturing the growth of the PBL during 0800–1300 LT but show significant differences after 1300 LT. Since the HRRR

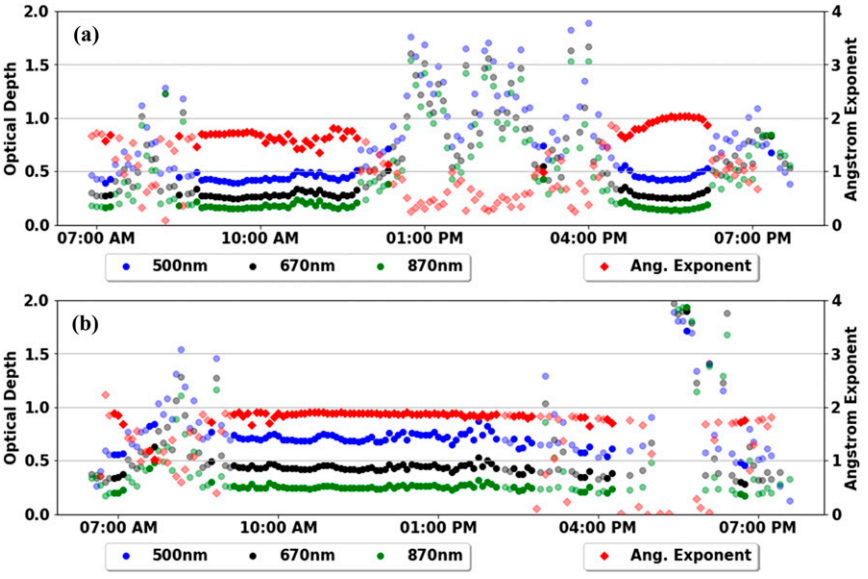

FIG. 14. Optical depth and Ångstrom exponent from eSIR at (a) Buffalo for 15 Aug and (b) Queens for 16 Aug 2018 (in local time) for three channels: 500, 670, and 870 nm. Bold color represents AOD, and light color represents cloud-contaminated optical depth.

model is based on potential temperature and sensible heat flux while the lidar method is based on aerosol backscatter, the discrepancies could be due to the different input parameters and scale. However, it is most likely that the HRRR overestimated the PBL height as all three lidar methods agree with one another and they closely match the radiosonde at 1900 LT. Similar to that at Buffalo, the gradient and variance methods at Queens (Fig. 16c) fail to detect PBL height correctly before 1000 LT and after 1600 LT due to the presence of multiple aloft aerosol layers. The WCT and HRRR show consistency in the PBL structure throughout the day. The HRRR model and radiosonde agree with each other at 0700 LT while all three lidar methods, the HRRR model and the radiosonde agree very well at 1900 LT. As demonstrated above, a profiler network provides an opportunity for accurate spatiotemporal monitoring of the PBL height across a large-scale region.

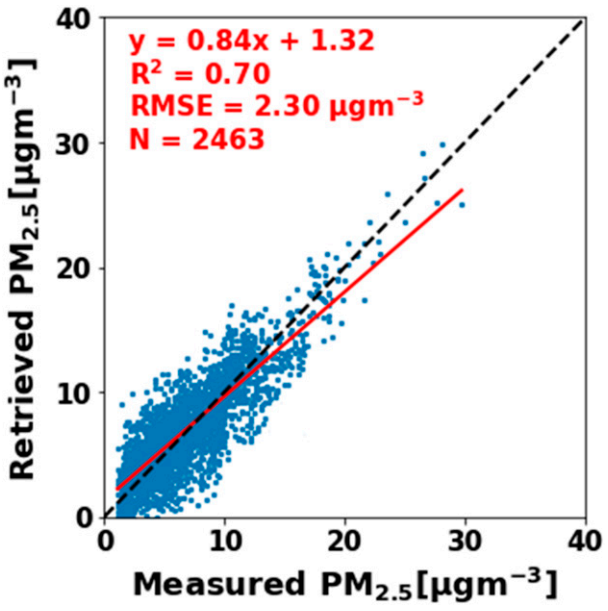

FIG. 15. Comparison of measured observations and nonlinear model–retrieved $PM_{2.5}$ at Queens during May–September 2020.

7. Summary and conclusions

The NYSM Profiler Network is a unique statewide observational network of 17 ground-based profiling stations. With a Doppler lidar, MWR and eSIR deployed at each site, atmospheric profile data (wind speed and direction, CNR, temperature, relative humidity, liquid, and vapor density) along with spectral direct, diffuse, and total radiation and fish-eye sky images are collected, archived, and disseminated every 10 min with the real-time graphics displayed at NYSM Profiler Network web page. The proximity of the NYSM Standard and Flux Network with the NYSM Profiler Network provides additional surface, soil, and energy budget data. Collectively, these real-time measurements yield valuable opportunities for monitoring and understanding key atmospheric exchange processes within the boundary layer and lower atmosphere. The network's high-spatial-resolution and high-temporal-resolution data within the PBL provide an important aid in understanding local heterogeneities across the state. Specifically, the NYSM Profiler Network allows for real-time monitoring of the sea breeze, long-range wildfire smoke transport, PBL height, and pollutants such as $PM_{2.5}$ that play important roles in local and regional weather and climate and air quality.

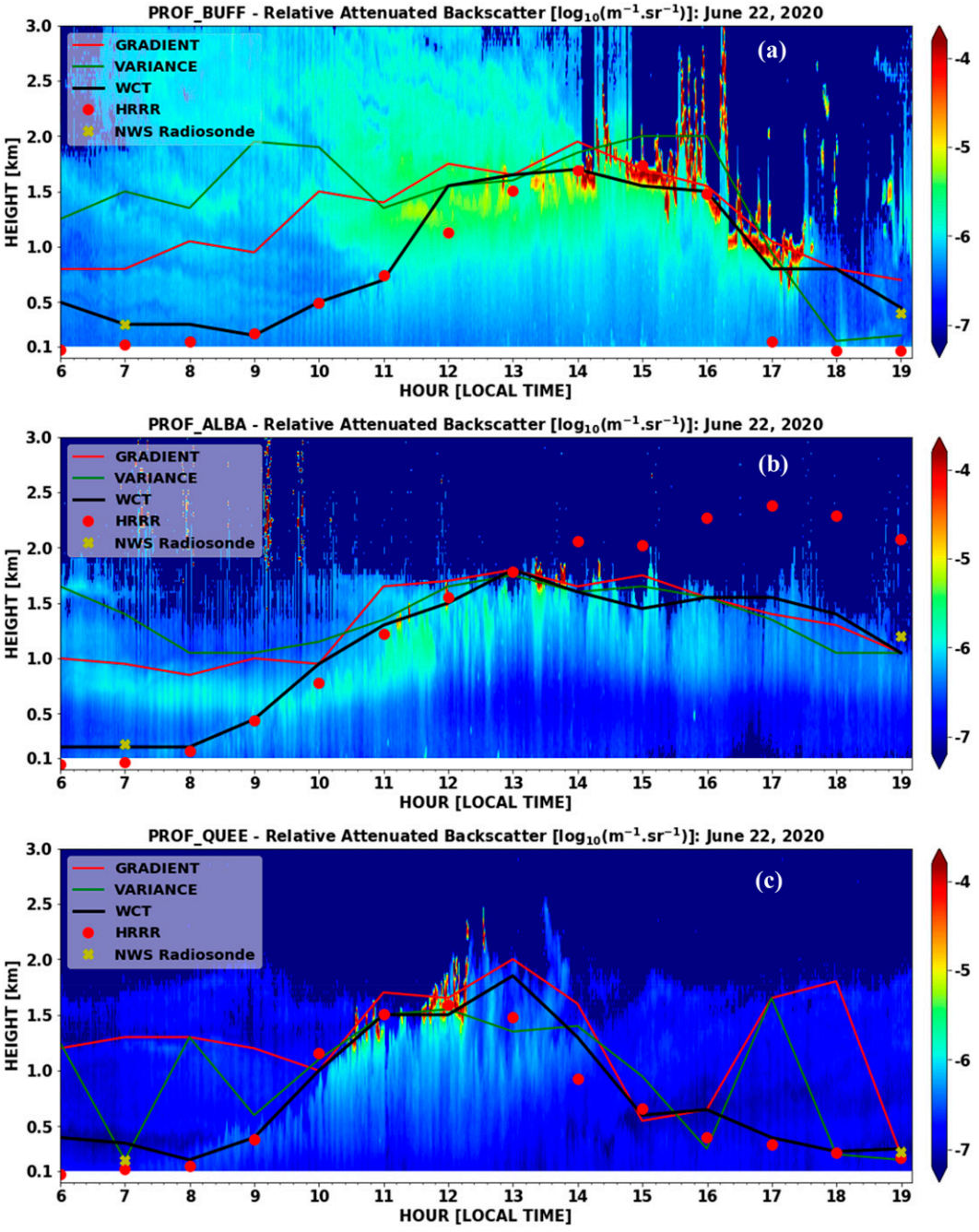

FIG. 16. The PBL retrieved from Doppler lidar at (a) Buffalo, (b) Albany, and (c) Queens along with data from the coincident NWS radiosonde and the HRRR model for 22 Jun 2020 (in local time).

The NYSM Profiler Network is foremost a research platform designed to address research questions through the assessment of profiles of kinematics and thermodynamics and optical depth variables with high temporal and spatial resolutions. For example, what is the optimal network density? What temporal resolution and configuration of sensors provides the greatest benefit? What value does such a system bring to NWP or weather operations? Observing system experiments (OSE) are currently under way to evaluate the benefit of assimilating ground-based profiler sensors data into numerical models. The monitoring of forecasting indices during high impact weather events has been demonstrated in B. Shrestha and E. Joseph (2021, unpublished manuscript).

The NYSM Profiler Network is now fully operational, distributing data to forecasters and researchers from across the state and to agencies such as the NWS and NASA. Such a

large-scale network offers a long-term and reliable platform for operations and research, bringing potential benefits to the weather, water, and climate enterprise for a wide variety of applications, including emergency management, renewable energy, aviation, and health.

Acknowledgments. This research is made possible by the New York State Mesonet (NYSM). Original funding for the NYSM was provided by Federal Emergency Management Agency Grant FEMA-4085-DR-NY, with the continued support of the NYS Division of Homeland Security and Emergency Services; the state of New York; the Research Foundation for the State University of New York (SUNY); the University at Albany, SUNY; the Atmospheric Sciences Research Center (ASRC) at SUNY Albany; and the Department of Atmospheric and Environmental Sciences (DAES) at SUNY Albany. The National Center for Atmospheric Research is sponsored by the National Science Foundation. Thanks are given to the University of Wyoming Department of Atmospheric Science for NWS radiosonde data, skew *T* plots, and upper-air maps; NWS Weather Prediction Center for the surface analysis map; New York State Department of Environmental Conservation (NYS DEC) for $PM_{2.5}$ data; and University of Utah for HRRR archive data. The authors declare that they have no real or perceived financial conflicts of interests.

Data availability statement. The NYSM Profiler Network data are available online (http://www.nysmesonet.org/weather/requestdata) subject to the NYSM data policy stated in the web page.

REFERENCES

Aitken, M. L., M. E. Rhodes, and J. K. Lundquist, 2012: Performance of a wind-profiling lidar in the region of wind turbine rotor disks. *J. Atmos. Oceanic Technol.*, **29**, 347–355, https://doi.org/10.1175/JTECH-D-11-00033.1.

Alexandrov, M. D., A. A. Lacis, B. E. Carlson, and B. Cairns, 2001: Remote sensing of atmospheric aerosols and trace gases by means of multifilter rotating shadowband radiometer. Part II: Climatological applications. *J. Atmos. Sci.*, **59**, 544–566, https://doi.org/10.1175/1520-0469(2002)059<0544:RSOAAA>2.0.CO;2.

——, A. Marshak, B. Cairns, A. A. Lacis, and B. E. Carlson, 2004: Automated cloud screening algorithm for MFRSR data. *Geophys. Res. Lett.*, **31**, L04118, https://doi.org/10.1029/2003GL019105.

——, A. A. Lacis, B. E. Carlson, and B. Cairns, 2008: Characterization of atmospheric aerosols using MFRSR measurements. *J. Geophys. Res.*, **113**, D08204, https://doi.org/10.1029/2007JD009388.

Ångström, A., 1929: On the transmission of sun radiation and on dust in the air. *Geogr. Ann.*, **2**, 156–166.

Baars, H., A. Ansmann, R. Engelmann, and D. Althausen, 2008: Continuous monitoring of the boundary layer top with lidar. *Atmos. Chem. Phys.*, **8**, 7281–7296, https://doi.org/10.5194/acp-8-7281-2008.

Bianco, L., K. Friedrich, J. M. Wilczak, D. Hazen, D. Wolfe, R. Delgado, S. P. Oncley, and J. K. Lundquist, 2017: Assessing the accuracy of microwave radiometers and radio acoustic sounding systems for wind energy applications. *Atmos. Meas. Tech.*, **10**, 1707–1721, https://doi.org/10.5194/amt-10-1707-2017.

Black, C., Y. Tesfaigzi, J. A. Bassein, and L. A. Miller, 2017: Wildfire smoke exposure and human health: Significant gaps in research for a growing public health issue. *Environ. Toxicol. Pharmacol.*, **55**, 186–195, https://doi.org/10.1016/j.etap.2017.08.022.

Blaylock, B. K., J. D. Horel, and E. T. Crosman, 2017a: Impact of lake breezes on summer ozone concentrations in the Salt Lake Valley. *J. Appl. Meteor. Climatol.*, **56**, 353–370, https://doi.org/10.1175/JAMC-D-16-0216.1.

——, ——, and S. T. Liston, 2017b: Cloud archiving and data mining of High-Resolution Rapid Refresh forecast model output. *Comput. Geosci.*, **109**, 43–50, https://doi.org/10.1016/j.cageo.2017.08.005.

Boquet, M., P. Royer, J. P. Cariou, and M. Machta, 2016: Simulation of Doppler lidar measurement range and data availability. *J. Atmos. Oceanic Technol.*, **33**, 977–987, https://doi.org/10.1175/JTECH-D-15-0057.1.

Brooks, I. M., 2003: Finding boundary layer top: Application of a wavelet covariance transform to lidar backscatter profiles. *J. Atmos. Oceanic Technol.*, **20**, 1092–1105, https://doi.org/10.1175/1520-0426(2003)020<1092:FBLTAO>2.0.CO;2.

Brotzge, J. A., and Coauthors, 2020: A technical overview of the New York State Mesonet standard network. *J. Atmos. Oceanic Technol.*, **37**, 1827–1845, https://doi.org/10.1175/JTECH-D-19-0220.1.

Cariou, J. P., L. Thobois, and P. Spencer, 2018: From Windcue#0001 to Windcube#1000: Doppler lidar as a mature technology. *19th Coherent Laser Radar Conf.*, Okinawa, Japan, TH14, http://clrccires.colorado.edu/data/paper/Th14.pdf.

Chudnovsky, A., A. Lyapustin, Y. Wang, C. Tang, J. Schwartz, and P. Koutrakis, 2014: High resolution aerosol data from MODIS satellite for urban air quality studies. *Cent. Eur. J. Geosci.*, **6**, 17–26, https://doi.org/10.2478/s13533-012-0145-4.

Cimini, D., and Coauthors, 2011: Thermodynamic atmospheric profiling during the 2010 Winter Olympics using ground-based microwave radiometry. *IEEE Trans. Geosci. Remote Sens.*, **49**, 4959–4969, https://doi.org/10.1109/TGRS.2011.2154337.

Delgado, R., and Coauthors, 2020: Unified ceilometer network. *MARAMA Air Monitoring Training Committee Workshop*, Mid Atlantic Regional Air Management Association, https://alg.umbc.edu/wp-content/uploads/2020/12/Delgado_Ceilometer_Network_update_MARAMA_2020_v2.pdf.

Eck, T. F., B. N. Holben, J. S. Reid, O. Dubovik, A. Smirnov, N. T. O'Neill, I. Slutsker, and S. Kinne, 1999: Wavelength dependence of the optical depth of biomass burning, urban and desert dust aerosols. *J. Geophys. Res.*, **104**, 31 333–31 349, https://doi.org/10.1029/1999JD900923.

Emami, F., M. Masiol, and P. K. Hopke, 2018: Air pollution at Rochester, NY: Long-term trends and multivariate analysis of upwind SO_2 source impacts. *Sci. Total Environ.*, **612**, 1506–1515, https://doi.org/10.1016/j.scitotenv.2017.09.026.

Flaherty, J. E., W. J. Shaw, J. M. Wilczak, A. B. White, C. W. King, and T. E. Ayers, 2016: DOE's 449 MHz wind profiling radars on the U.S. West Coast: Annual summary for fiscal year 2016. U.S. DOE Rep. PNNL-25925, 30 pp., https://www.pnnl.gov/main/publications/external/technical_reports/PNNL-25925.pdf.

Flentje, H., B. Heese, J. Reichardt, and W. Thomas, 2010: Aerosol profiling using the ceilometer network of the German

Meteorological Service. *Atmos. Meas. Tech.*, **3**, 3643–3673, https://doi.org/10.5194/amtd-3-3643-2010.

Ford, B., M. Val Martin, S. E. Zelasky, E. V. Fischer, S. C. Anenberg, C. L. Heald, and J. R. Pierce, 2018: Future fire impacts on smoke concentrations, visibility, and health in the contiguous United States. *Geohealth*, **2**, 229–247, https://doi.org/10.1029/2018GH000144.

Granados-Munoz, M. J., F. Navas-Guzman, J. A. Bravo-Aranda, J. L. Guerrero-Rascado, H. Lyamani, J. Fernandez-Galvez, and L. Albados-Arboledas, 2012: Automatic determination of the planetary boundary layer height using lidar: One-year analysis over southeastern Spain. *J. Geophys. Res.*, **117**, D18208, https://doi.org/10.1029/2012JD017524.

Güldner, J., and D. Spänkuch, 2001: Remote sensing of the thermodynamic state of the atmospheric boundary layer by ground-based microwave radiometry. *J. Atmos. Oceanic Technol.*, **18**, 925–933, https://doi.org/10.1175/1520-0426(2001)018<0925:RSOTTS>2.0.CO;2.

Gupta, P., and S. A. Christopher, 2008: Seven year particulate matter air quality assessment from surface and satellite measurements. *Atmos. Chem. Phys.*, **8**, 3311–3324, https://doi.org/10.5194/acp-8-3311-2008.

Hansen, J. E., and L. D. Travis, 1974: Light scattering in planetary atmospheres. *Space Sci. Rev.*, **16**, 527–610, https://doi.org/10.1007/BF00168069.

Heffter, J. L., 1980: Transport layer depth calculations. *Second Joint Conf. on Applications of Air Pollution Meteorology*, New Orleans, LA, Amer. Meteor. Soc., 787–791.

Hewison, T., 2007: 1D-VAR retrievals of temperature and humidity profiles from a ground-based microwave radiometer. *IEEE Trans. Geosci. Remote Sens.*, **45**, 2163–2168, https://doi.org/10.1109/TGRS.2007.898091.

——, and C. Gaffard, 2003: Radiometrics MP3000 microwave radiometer performance assessment version 1.0. Met Office Observations Development Tech. Rep.-TR29, 43 pp., http://tim.hewison.org/TR29.pdf.

Hill, C., 2018: Coherent focused lidars for Doppler sensing of aerosols and wind. *Remote Sens.*, **10**, 466, https://doi.org/10.3390/rs10030466.

Hu, X., and Coauthors, 2013: Estimating ground-level $PM_{2.5}$ concentrations in the southeastern U.S. using geographically weighted regression. *Environ. Res.*, **121**, 1–10, https://doi.org/10.1016/j.envres.2012.11.003.

Hua, Z., W. Sun, G. Yang, and Q. Du, 2019: A full coverage daily average $PM_{2.5}$ retrieval method with two stage IVW fused MODIS C6 AOD and two stage GAM model. *Remote Sens.*, **11**, 1558, https://doi.org/10.3390/rs11131558.

Hung, W.-T., and Coauthors, 2020: The impacts of transported wildfire smoke aerosols on surface air quality in New York State: A case study in summer 2018. *Atmos. Environ.*, **227**, 117415, https://doi.org/10.1016/j.atmosenv.2020.117415.

Illingworth, A. J., and Coauthors, 2019: How can existing ground-based profiling instruments improve European weather forecasts? *Bull. Amer. Meteor. Soc.*, **100**, 605–619, https://doi.org/10.1175/BAMS-D-17-0231.1.

Joseph, E., B. Shrestha, C. Conover, B. Stutsrim, M. J. Schwab, J. J. Schwab, and J. Zhang, 2018: Ozone sonde measurements from Flax Pond, Long Island during the 2018 LISTOS Field Intensive. *AGU Fall Meeting*, Washington, DC, Amer. Geophys. Union, Abstract A51N-2402.

Kassianov, E. I., J. C. Barnard, and T. P. Ackerman, 2005: Retrieval of aerosol microphysical properties using surface MultiFilter Rotating Shadowband Radiometer (MFRSR) data: Modeling and observations. *J. Geophys. Res.*, **110**, D09201, https://doi.org/10.1029/2004JD005337.

Knupp, K. R., R. Ware, D. Cimini, F. Vandenberghe, J. Vivekanandan, E. Westwater, T. Coleman, and D. Phillips, 2008: Ground-based passive microwave profiling during dynamic weather conditions. *J. Atmos. Oceanic Technol.*, **26**, 1057–1073, https://doi.org/10.1175/2008JTECHA1150.1.

Kollias, P., and Coauthors, 2020: The ARM Radar Network: At the leading edge of cloud and precipitation observations. *Bull. Amer. Meteor. Soc.*, **101**, E588–E607, https://doi.org/10.1175/BAMS-D-18-0288.1.

Koontz, A., G. Hodges, J. Barnard, C. Flynn, and J. Michalsky, 2013: Aerosol Optical Depth Value-Added Product. U.S. DOE Rep. DOE/SC-ARM/TR-129, 32 pp., https://www.arm.gov/publications/tech_reports/doe-sc-arm-tr-129.pdf.

Koskinen, J. T., and Coauthors, 2011: The Helsinki Testbed: A mesoscale measurement, research and service platform. *Bull. Amer. Meteor. Soc.*, **92**, 325–342, https://doi.org/10.1175/2010BAMS2878.1.

Kucher, N., D. D. Turner, U. Lohnert, and S. Crewell, 2016: Calibrating ground-based microwave radiometer: Uncertainty and drifts. *Radio Sci.*, **51**, 311–327, https://doi.org/10.1002/2015RS005826.

Kumer, V. M., J. Reuder, and B. R. Furevik, 2014: A comparison of LiDAR and radiosonde wind measurements. *Energy Procedia*, **53**, 214–220, https://doi.org/10.1016/j.egypro.2014.07.230.

Laroche, S., and R. Sarrazin, 2013: Impact of radiosonde balloon drift on numerical weather prediction and verification. *Wea. Forecasting*, **28**, 772–782, https://doi.org/10.1175/WAF-D-12-00114.1.

Lee, J., and Coauthors, 2019: Ceilometer monitoring of boundary-layer height and its application in evaluating the dilution effect on air pollution. *Bound.-Layer Meteor.*, **172**, 435–455, https://doi.org/10.1007/s10546-019-00452-5.

Liljegren, J. C., 2002: Evaluation of a new multi-frequency microwave radiometer for measuring the vertical distribution of temperature, water vapor, and cloud liquid water. *DOE ARM Program Tech. Rep.*, 67 pp.

——, B. M. Lesht, S. Kato, and E. E. Clothiaux, 2001: Initial evaluation of profiles of temperature, water vapor and cloud liquid water from a new microwave radiometer. *11th ARM Science Team Meeting Proc.*, Atlanta, GA, U.S. Department of Energy, https://www.arm.gov/publications/proceedings/conf11/extended_abs/liljegren_jc.pdf.

Liu, J. C., and Coauthors, 2016: Particulate air pollution from wildfires in the western US under climate change. *Climatic Change*, **138**, 655–666, https://doi.org/10.1007/s10584-016-1762-6.

Loughner, C. P., and Coauthors, 2014: Impact of bay-breeze circulations on surface air quality and boundary layer export. *J. Appl. Meteor. Climatol.*, **53**, 1697–1713, https://doi.org/10.1175/JAMC-D-13-0323.1.

Munkel, C., 2006: Boundary layer and air quality monitoring with a commercial lidar ceilometer. *Proc. SPIE*, **6367**, 63670Q, https://doi.org/10.1117/12.689775.

NASA, 2019: Earth Science and Applications Decadal Survey. NASA, 47 pp., https://science.nasa.gov/science-red/s3fs-public/atoms/files/ESD Community Forum - March 4 2019 - FINAL.pdf.

National Research Council, 2009: *Observing Weather and Climate from the Ground Up: A Nationwide Network of Networks*. National Academies Press, https://doi.org/10.17226/12540.

Newman, J. F., P. M. Klein, S. Wharton, A. Sathe, T. A. Bonin, P. B. Chilson, and A. Muschinski, 2016: Evaluation of three

lidar scanning strategies for turbulence measurements. *Atmos. Meas. Tech.*, **9**, 1993–2013, https://doi.org/10.5194/amt-9-1993-2016.

North, K. W., M. Oue, P. Kollias, S. E. Giangrande, S. M. Collis, and C. K. Potvin, 2017: Vertical air motion retrievals in deep convective clouds using the ARM scanning radar network in Oklahoma during MC3E. *Atmos. Meas. Tech.*, **10**, 2785–2806, https://doi.org/10.5194/amt-10-2785-2017.

Patadia, F., R. C. Levy, and S. Mattoo, 2018: Correcting for trace gas absorption when retrieving aerosol optical depth from satellite observations of reflected shortwave radiation. *Atmos. Meas. Tech.*, **11**, 3205–3219, https://doi.org/10.5194/amt-11-3205-2018.

Radiometrics, 2013: Profiler operator's manual. Radiometrics Corporation Doc., 197 pp., http://radiometrics.com/data/uploads/2014/08/MP-3000A-Operator-Manual-RevG.pdf.

Rattigan, O. V., K. L. Civerolo, H. D. Felton, J. J. Schwab, and K. L. Demerjian, 2015: Long term trends in New York: $PM_{2.5}$ mass and particle components. *Aerosol Air Qual. Res.*, **16**, 1191–1205, https://doi.org/10.4209/aaqr.2015.05.0319.

Rogers, H. M., J. C. Ditto, and D. R. Gentner, 2020: Evidence for impacts on surface level air quality in northeastern US from long-distance transport of smoke from North American fires during the Long Island Sound Tropospheric Ozone Study (LISTOS) 2018. *Atmos. Chem. Phys.*, **20**, 671–682, https://doi.org/10.5194/acp-20-671-2020.

Royer, P., M. Boquet, J.-P. Cariou, L. Sauvage, and R. Parmentier, 2016: Aerosol/cloud measurements using coherent wind Doppler lidars. *EPJ Web Conf.*, **119**, 11002, https://doi.org/10.1051/epjconf/201611911002.

Schaap, M., A. Apituley, R. M. A. Timmermans, R. B. A. Koelemeijer, and G. de. Leeuw, 2009: Exploring the relationship between aerosol optical depth and PM2.5 at Cabauw, the Netherlands. *Atmos. Chem. Phys.*, **9**, 909–925, https://doi.org/10.5194/acp-9-909-2009.

Schlatter, T., 2004: Cost and operational effectiveness analysis for the NOAA Profiler Network. NOAA Tech. Memo. OAR GSD-56, 108 pp., https://doi.org/10.7289/V5/TM-OAR-GSD-56.

Schroeder, J., and E. Westwater, 1991: User's guide to WPL microwave radiative transfer software. NOAA Tech. Memo. ERL WPL-213, 84 pp.

Schuster, G. L., O. Dubovik, and B. N. Holben, 2006: Angstrom exponent and bimodal aerosol size distributions. *J. Geophys. Res.*, **111**, D07207, https://doi.org/10.1029/2005JD006328.

Sivaraman, C., S. McFarlane, E. Chapman, M. Jensen, T. Toto, S. Liu, and M. Fischer, 2013: Planetary boundary layer height (PBL) value added product (VAP): Radiosonde retrievals. U.S. DOE Tech. Rep. DOE/SC-ARM/TR-132, 36 pp., https://www.arm.gov/publications/tech_reports/doe-sc-arm-tr-132.pdf.

Solheim, F., J. Godwin, E. Westwater, Y. Han, S. Keihm, K. Marsh, and R. Ware, 1998: Radiometric profiling of temperature, water vapor, and cloud liquid water using various inversion methods. *Radio Sci.*, **33**, 393–404, https://doi.org/10.1029/97RS03656.

Strauch, R. G., D. A. Merritt, K. P. Moran, K. B. Earnshaw, and D. Kamp, 1983: The Colorado Wind Profiling Network. *J. Atmos. Oceanic Technol.*, **1**, 37–49, https://doi.org/10.1175/1520-0426(1984)001<0037:TCWPN>2.0.CO;2.

Suomi, I., S. E. Gryning, E. J. O'Connor, and T. Vihma, 2017: Methodology for obtaining wind gusts using Doppler lidar. *Quart. J. Roy. Meteor. Soc.*, **143**, 2061–2072, https://doi.org/10.1002/qj.3059.

Turner, D. D., S. A. McFarlane, L. Riihimaki, Y. Shi, C. Lo, and Q. Min, 2014: Cloud optical properties from the multifilter shadowband radiometer (MFRSRCLDOD): An ARM value-added product. U.S. DOE Tech. Rep. DOE/SC-ARM/TR-139, 29 pp., https://www.osti.gov/servlets/purl/1237958.

Wagner, T. J., P. M. Klein, and D. D. Turner, 2019: A new generation of ground based mobile platforms for active and passive profiling of the boundary layer. *Bull. Amer. Meteor. Soc.*, **100**, 137–153, https://doi.org/10.1175/BAMS-D-17-0165.1.

Wilczak, J. M., E. E. Gossard, W. D. Neff, and W. L. Eebrehard, 1996: Ground based remote sensing of the atmospheric boundary layer: 25 years of progress. *Bound.-Layer Meteor.*, **71**, 277–296, https://doi.org/10.1007/978-94-017-0944-6_14.

WMO, 2018: Statement of guidance for high-resolution numerical weather prediction (NWP). WMO Rep., 12 pp., http://www.wmo.int/pages/prog/www/OSY/SOG/SoG-HighRes-NWP.pdf.

Wu, Y., A. Arapi, J. Huang, B. Gross, and F. Moshary, 2018: Intra-continental wildfire smoke transport and impact on local air quality observed by ground-based and satellite remote sensing in New York City. *Atmos. Environ.*, **187**, 266–281, https://doi.org/10.1016/j.atmosenv.2018.06.006.

Yang, S., J. Preißler, M. Wiegner, S. Löwis, G. N. Petersen, M. M. Parks, and D. C. Finger, 2020: Monitoring dust events using Doppler lidar and ceilometer in Iceland. *Atmosphere*, **11**, 1294, https://doi.org/10.3390/atmos11121294.

Yin, B., Q. Min, and E. Joseph, 2015: Retrievals and uncertainty analysis of aerosol single scattering albedo from MFRSR measurements. *J. Quant. Spectrosc. Radiat. Transfer*, **150**, 95–106, https://doi.org/10.1016/j.jqsrt.2014.08.012.

Zhang, J., M. Ninneman, E. Joseph, M. J. Schwab, B. Shrestha, and J. Schwab, 2020: Mobile laboratory measurements of high surface ozone levels and spatial heterogeneity during LISTOS 2018: Evidence for sea breeze influence. *J. Geophys. Res. Atmos.*, **125**, e2019JD031961, https://doi.org/10.1029/2019JD031961.